DISK ASSEMBLY AND THE $M_{BH} - \sigma_e$ RELATION OF SUPERMASSIVE BLACK HOLES

Victor P. Debattista[1,2], Stelios Kazantzidis[3], Frank C. van den Bosch[4,5]

Unfinished draft January 15, 2013

ABSTRACT

Recent Hubble Space Telescope (*HST*) observations have revealed that a majority of active galactic nuclei (AGN) at $z \sim 1-3$ are resident in isolated disk galaxies, contrary to the usual expectation that AGN are triggered by mergers. Here we develop a new test of the cosmic evolution of supermassive black holes (SMBHs) in disk galaxies by considering the local population of SMBHs. We show that substantial SMBH growth in spiral galaxies is *required* as disks assemble. SMBHs exhibit a tight relation between their mass and the velocity dispersion of the spheroid within which they reside, the $M_\bullet - \sigma_e$ relation. In disk galaxies the bulge is the spheroid of interest. We explore the evolution of the $M_\bullet - \sigma_e$ relation when bulges form together with SMBHs on the $M_\bullet - \sigma_e$ relation and then slowly reform a disk around them. The formation of the disk compresses the bulge raising its σ_e. We present evidence for such compression in the form of larger velocity dispersion of classical bulges compared with elliptical galaxies at the same mass. This compression leads to an offset in the $M_\bullet - \sigma_e$ relation if it is not accompanied by an increased $M_\bullet$. We quantify the expected offset based on photometric data and show that, on average, SMBHs must grow by $\sim 50-65\%$ just to remain on the $M_\bullet - \sigma_e$ relation. We find no significant offset in the $M_\bullet - \sigma_e$ relations of classical bulges and of ellipticals, implying that SMBHs have been growing along with disks. Our simulations demonstrate that SMBH growth is *necessary* for the local population of disk galaxies to have remained on the $M_\bullet - \sigma_e$ relation.

Subject headings: black hole physics — galaxies: bulges — galaxies: evolution — galaxies: nuclei — cosmology: theory — methods: numerical

1. INTRODUCTION

The energetics and demographics of active galactic nuclei (AGN), which are found already by $z = 6$ (Zheng et al. 2000; Fan et al. 2000, 2004, 2006), can be explained by the presence of accreting supermassive black holes (Lynden-Bell 1969; Soltan 1982; Chokshi & Turner 1992; Salucci et al. 1999; Merritt & Ferrarese 2001a). The *Hubble Space Telescope* (*HST*) has revealed such supermassive black holes (SMBHs), with masses in the range $10^6 - 10^9 M_\odot$, in a number of nearby quiescent galaxies (Kormendy & Richstone 1995). However the formation and growth of SMBHs remains something of a mystery with a variety of models proposed (Madau & Rees 2001; Portegies Zwart & McMillan 2002; Miller & Hamilton 2002; Oh & Haiman 2002; Volonteri et al. 2003; Islam et al. 2003; Koushiappas et al. 2004; Hopkins et al. 2006; Volonteri & Rees 2005; Begelman et al. 2006; Lodato & Natarajan 2006; King & Pringle 2006; Mayer et al. 2010).

SMBHs exhibit a number of scaling relations, the tightest of which is the $M_\bullet - \sigma_e$ relation between their mass, $M_\bullet$, and the velocity dispersion, σ_e, of the spheroids within which they reside. A scaling-relation of the form $\log M_\bullet = \alpha + \beta \log(\sigma_e/200 \mathrm{~km\,s^{-1}})$ was found by Gebhardt et al. (2000) and Ferrarese & Merritt (2000). Early measurements of the slope β varied from 4.02 ± 0.32 (Tremaine et al. 2002) to 4.72 ± 0.36 (Merritt & Ferrarese 2001b). More recent measurements still find a large range of β spanning $\beta = 4.24 \pm 0.41$ (Gültekin et al. 2009) to $\beta = 5.57 \pm 0.33$ (McConnell et al. 2011; McConnell & Ma 2012). Other suggested correlations between SMBHs and their host bulges include the $M_\bullet - L_{bul}$ or $M_\bullet - M_{bul}$ relations with the bulge luminosity or mass (Kormendy & Richstone 1995; Magorrian et al. 1998; Marconi & Hunt 2003; Häring & Rix 2004), and the $M_\bullet - n$ relation with the bulge Sérsic index (Graham & Driver 2007). A three-parameter fundamental plane for SMBHs has also been suggested (Marconi & Hunt 2003; de Francesco et al. 2006; Aller & Richstone 2007; Hopkins et al. 2007b,a; Barway & Kembhavi 2007). Graham (2008) argued that the fundamental plane is caused by barred galaxies. Beifiori et al. (2012) found that the fundamental plane is strongly dominated by σ_e. A relation between $M_\bullet$ and M_{gal}, the mass of the host galaxy, has been suggested (Ferrarese 2002; Baes et al. 2003; Pizzella et al. 2005). Early work found that the same relation is satisfied also by nuclear star clusters (Ferrarese et al. 2006; Wehner & Harris 2006; Rossa et al. 2006), which may provide a unified picture of the growth of central massive objects (McLaughlin et al. 2006; Hartmann et al. 2011). However more recent work has found that nuclear star clusters and SMBHs follow different scaling relations (Erwin & Gadotti 2012a; Leigh et al. 2012;

[1] RCUK Fellow, Jeremiah Horrocks Institute, University of Central Lancashire, Preston, PR1 2HE, UK vpdebattista@gmail.com
[2] Visiting Lecturer, Department of Physics, University of Malta, Tal-Qroqq Street, Msida, MSD 2080, Malta
[3] Center for Cosmology and Astro-Particle Physics; and Department of Physics; and Department of Astronomy, The Ohio State University, Columbus, OH 43210, USA; stelios@mps.ohio-state.edu
[4] Astronomy Department, Yale University, PO Box 208101, New Haven, CT 06520-8101, USA frank.vandenbosch@yale.edu
[4] Lady Davis Visiting Professor, Racah Institute of Physics, Hebrew University, Jerusalem 91904, Israel

Scott & Graham 2012). This may possibly be a result of the scaling relations being different in late-type galaxies (Greene et al. 2010; Erwin & Gadotti 2012b).

The clues to SMBH growth and formation implied by these scaling relations are non-trivial to decipher: The sphere of influence of a typical SMBH has a radius of a few parsecs, which is some 2-3 orders of magnitude smaller than the effective radius of a typical bulge. What mechanism then gives rise to these scaling relations? Do SMBHs regulate bulge growth or is the growth of SMBHs restricted by the bulge in which they reside? Examples of the latter are scenarios in which gas accretion onto the SMBH is regulated by star formation (Burkert & Silk 2001; Kazantzidis et al. 2005; Zheng et al. 2009), or by stellar feeding of SMBH accretion disks (Miralda-Escudé & Kollmeier 2005). AGN feedback via heating, pressure-driven winds or ionization typically gives rise to scenarios in which SMBHS regulate their own or bulge growth (Silk & Rees 1998; Wyithe & Loeb 2003; King 2003; Murray et al. 2005; Di Matteo et al. 2005; Sazonov et al. 2005; Younger et al. 2008). High velocity outflows that may be associated with such AGN feedback have been observed in Seyfert 1 galaxies (e.g. Crenshaw et al. 1999). In addition, in semi-analytic models, AGN feedback is often invoked to explain the high mass end of the luminosity function (Croton et al. 2006; Bower et al. 2006). Alternatively, collapse models in which the $M_\bullet - \sigma_e$ relation is an indirect consequence of unrelated processes have also been proposed (Haehnelt & Kauffmann 2000; Adams et al. 2001, 2003; Peng 2007; Volonteri & Natarajan 2009; Jahnke & Macciò 2011).

One of the characteristics of the scaling relations is that $M_\bullet$ correlates with the properties of the host *spheroid*. In disk galaxies this is the bulge component. Bulges in disk galaxies come in two types: "classical" and "pseudo" bulges, with mixed types also possible (e.g. Erwin et al. 2003; Debattista et al. 2005; Athanassoula 2005; Nowak et al. 2010). Classical bulges are believed to form via merging of sub-galactic clumps, satellites and clusters (Eggen et al. 1962; Tremaine et al. 1975; Searle & Zinn 1978; Kauffmann et al. 1993; Baugh et al. 1996; van den Bosch 1998). In essence classical bulges are elliptical galaxies around which a disk has reformed (e.g. Steinmetz & Navarro 2002) although continued late growth of classical bulges is also possible (e.g. Hopkins et al. 2010). Pseudo bulges instead are formed by the secular evolution of disk structure, such as bars and spirals (Combes & Sanders 1981; Combes et al. 1990; Raha et al. 1991; Norman et al. 1996; Courteau et al. 1996; Bureau & Freeman 1999; Debattista et al. 2004; Athanassoula 2005; Drory & Fisher 2007). Kormendy & Kennicutt (2004) reviewed the observational evidence for pseudo bulge formation. In contrast to pseudo bulges, classical bulges form early, predating the formation of the disk. The difference between classical and pseudo bulges is reflected also in their SMBH demographics. Gadotti & Kauffmann (2009) estimate that classical bulges account for 41% of the black hole mass in the local universe, while pseudo bulges host only 4%. Gültekin et al. (2009) find that the classical bulges (including elliptical galaxies) follow the same $M_\bullet - \sigma_e$

relation as the general population, with a scatter of 0.45 ± 0.066. Instead Hu (2008) found that pseudo bulges have an $M_\bullet - \sigma_e$ relation with the same slope as, but lower zero-point than, classical bulges. Greene et al. (2010) showed that the SMBHs of late-type galaxies, which predominantly contain pseudo bulges, scatter below the $M_\bullet - \sigma_e$ relation.

A number of studies using simulations have explored the evolution of the $M_\bullet - \sigma_e$ relation during hierarchical merging (e.g. Kazantzidis et al. 2005; Springel et al. 2005a,b; Younger et al. 2008; Johansson et al. 2009; Robertson et al. 2006). However, recent *HST* observations have shown that a surprisingly substantial fraction of AGN activity at high redshifts is associated with isolated disk galaxies, rather than with mergers. Schawinski et al. (2011) show that $\sim 80\%$ of X-ray-selected AGN at $z = 1.5-3$ are in low Sérsic-index galaxies, indicative of disks. They find that moderate luminosity AGN hosts at $z \sim 2$ are similar to those at $z \sim 0$. Excluding the high luminosity quasars, which are triggered by mergers (Treister et al. 2010), they estimate that $23-40\%$ of SMBH growth occurs in intermediate brightness Seyfert AGN. The X-ray-selected sample of moderate-luminosity AGN at $1.5 < z < 2.5$ of Cisternas et al. (2011) consists of more than 50% disk galaxies, with ongoing mergers evident no more frequently than in non-active galaxies. Schawinski et al. (2012) show that even heavily obscured quasars are hosted largely by disks, not by mergers. Studies of star-formation using *Herschel* find that the specific star formation rates of X-ray selected AGN hosts are no different from those of inactive galaxies, also indicating that AGN hosts are not undergoing fundamentally different behaviors (Mullaney et al. 2012b,a). Using multiwavelength surveys of AGN across redshifts $0 \leq z \leq 3$ Treister et al. (2012) found that only the most luminous AGN phases are connected to major mergers, the rest being driven by secular processes. The merger driven AGN activity accounts for only $\sim 10\%$ of AGN. The "anti-hierarchical" nature of galaxy and AGN growth — both the largest galaxies (Bower et al. 1992; Thomas et al. 2005; Nelan et al. 2005) and the brightest AGN (Ueda et al. 2003; Hasinger et al. 2005) form at high redshift whereas lower mass galaxies and moderate luminosity AGN peak at lower redshifts — also hints that internal evolution rather than mergers is the main driver of SMBH growth. AGN activity continues to be dominated by disk galaxies down to the present: since $z \sim 1$ more than 85% of AGN activity is hosted in galaxies with no evidence of recent mergers (Kocevski et al. 2012). Lastly, the presence of AGN in bulgeless galaxies, which are thought to not have experienced much hierarchical merging, provides further evidence that internal evolution is capable of driving SMBH growth (Simmons et al. 2012; Araya Salvo et al. 2012).

This paper introduces a novel approach to exploring the origin of the $M_\bullet - \sigma_e$ relation. We study the consequences of disk regrowth for the $M_\bullet - \sigma_e$ relation of classical bulges under the assumption that a classical bulge forms with a SMBH satisfying the $M_\bullet - \sigma_e$ relation and then a disk reassembles around it. Growth of the disk then compresses the bulge (Andredakis 1998). Since σ_e is not an adiabatic invariant, compression leads to its evolution, which we quantify here. We study the effect of this evolution on the $M_\bullet - \sigma_e$ relation. If SMBHs

remain on the $M_\bullet - \sigma_e$ relation then this implies that SMBH growth is governed by the potential (as characterized by σ_e) within which they sit, which is most likely if AGN feedback regulates SMBH growth. If instead we find that bulges evolve away from the $M_\bullet - \sigma_e$ relation, with the SMBHs retaining a memory of the bulge within which they formed, then this implies that bulge growth is limited by the SMBH, as would happen if AGN feedback quenches star formation in the bulge. The paper is organized as follows. Section 2 describes the simulation methods used in this paper. Section 3 presents the evolution of σ_e caused by disk (re-)assembly and derives a photometric estimate for the increase in σ_e. In Section 4 we predict the consequences of bulge compression for the $M_\bullet - \sigma_e$ relation. We find that the main effect is a shift to lower mass in the zero-point of the relation. Then in Section 5 we test this prediction on observational data. We find no evidence for such a shift, indicating that SMBHs have grown along with disks. We show that the degree by which SMBHs must have grown is consistent with the new *HST* estimates. Section 6 sums up our results.

2. NUMERICAL SIMULATIONS

We construct initially spherically symmetric two-component galaxy models consisting of a stellar bulge embedded in an extended dark matter (DM) halo. For the DM component, we consider the cuspy, cosmologically-motivated Navarro et al. (1996, hereafter NFW) density profile given by

$$\rho_{DM}(r) = \frac{\rho_s}{(r/r_s)(1 + r/r_s)^2} \qquad (r \leq r_{vir}), \qquad (1)$$

where ρ_s is a characteristic inner density, r_s denotes the scale radius of the density profile defined as the distance from the center where the logarithmic slope, $d\ln\rho(r)/d\ln r$, is equal to -2, and r_{vir} is the virial radius defined as the radius enclosing an average density equal to the virial overdensity times the critical density for a flat universe. We adopt the ΛCDM concordance cosmology with $\Omega_m = 0.3$, $\Omega_\Lambda = 0.7$, and $h = 0.7$, and assume $z = 0$. The virial overdensity is then equal to $\Delta_{vir} \simeq 103.5$ (e.g., Lacey & Cole 1993).

The NFW density profile is formally infinite in extent with a cumulative mass that diverges as $r \to \infty$. In order to keep the total mass finite, we implement an exponential cutoff which sets in at the virial radius and turns off the profile on a scale r_{decay}. The truncation scale r_{decay} is a free parameter and controls the sharpness of the transition. Explicitly, we model the density profile beyond r_{vir} by

$$\rho(r) = \frac{\rho_s}{c(1+c)^2}\left(\frac{r}{r_{vir}}\right)^\kappa \exp\left[-\frac{r - r_{vir}}{r_{decay}}\right] (r > r_{vir}), \qquad (2)$$

where $c \equiv r_{vir}/r_s$ is the concentration parameter and κ is fixed by the requirement that $d\ln\rho(r)/d\ln r$ is continuous at r_{vir}. This procedure is necessary because sharp truncations result in models that are not in equilibrium (Kazantzidis et al. 2004). For the purposes of the present study, we adopt a concentration parameter $c = 10$, appropriate for Milky Way Galaxy-sized dark matter halos (Bullock et al. 2001), and a truncation scale $r_{decay} = 0.1r_s$.

For the spatial distribution of the bulge component, we adopt the de-projected Sérsic law (Sérsic 1968) of Simonneau & Prada (2004):

$$\rho(s) = \rho_0 \int_0^1 \frac{\exp\left[-ks^{\frac{1}{n}}(1 - x^2)^{-\frac{1}{n-1}}\right]}{1 - (1 - x^2)^{\frac{n}{n-1}}} x \, dx \qquad (n > 1), \qquad (3)$$

where

$$\rho_0 = \frac{k}{\pi} \frac{\Sigma_0}{R_{e,0}} \frac{2}{n-1} \frac{1}{s^{\frac{n-1}{n}}}. \qquad (4)$$

In the above equations, n denotes the Sérsic index, $R_{e,0}$ is the effective radius, *i.e.* the radius that encloses half the total projected luminosity, Σ_0 is the central value of the projected mass profile, and $s \equiv r/R_{e,0}$. For $n \geq 1$, k can be estimated (with an error smaller than 0.1%) by the relation $k = 2n - 0.324$ (Ciotti 1991). Our initial bulge has Sérsic index $n = 4$, *i.e.* it is characterized by a de Vaucouleurs (1948) profile. For the specific galaxy model we consider, the ratio between the mass of the bulge and the *virial* mass of the halo is equal to 8×10^{-3}, while the ratio between the bulge effective radius and the halo scale radius, $R_{e,0}/r_s = 0.02$. Our standard scaling has $R_{e,0} = 500$ pc and bulge mass $M_b = 8 \times 10^9$ M$_\odot$, leading to $r_{vir} = 270$ kpc and $M_{vir} = 10^{12}$M$_\odot$. Because we do not consider non-gravitational processes such as gaseous dissipation, the scale-free nature of gravity allows the rescaling of our models.

Monte-Carlo realizations of the N-body galaxy model are constructed according to the procedure described in Kazantzidis et al. (2004), which is based on sampling the exact phase-space distribution function (DF). Under the assumption of isotropy, the DF of each component depends only on the binding energy per unit mass E:

$$f_i(E) = \frac{1}{\sqrt{8}\pi^2}\left[\int_0^E \frac{d^2\rho_i}{d\Psi^2} \frac{d\Psi}{\sqrt{E - \Psi}} + \frac{1}{\sqrt{E}}\left(\frac{d\rho_i}{d\Psi}\right)_{\Psi=0}\right], \qquad (5)$$

where ρ_i is the density profile of component i and $\Psi(r) = \psi_{DM}(r) + \psi_{stars}(r)$ is the total *relative* gravitational potential. Note that the second term on the right-hand side in Eqn. 5 vanishes for any sensible behavior of $\Psi(r)$ and $\rho_i(r)$ as $r \to \infty$.

The system generated this way needs to be softened; the gravitational softening lengths are set to $\epsilon = 15$ pc for all particles (including the disk particles described below) in all runs. Since softening the potential is equivalent to smoothing the density distribution (Barnes 2012), the initial conditions set up without softening are not a perfect equilibrium. We therefore relax the initial bulge+halo system for 250 Myr before we start growing the disk. During this period the bulge settles to a new equilibrium. For the remainder of this paper we refer to this relaxed model as the initial conditions.

After the bulge+halo system has reached equilibrium, we investigate its response to the growth of various external disk fields. The growing disks follow an exponential distribution in cylindrical radius R, and their structure is modeled as (Spitzer 1942; Freeman 1970):

$$\rho_d(R, z, t) = \frac{m_d(t)}{8\pi z_d R_d^2} \exp\left(-\frac{R}{R_d}\right) \text{sech}^2\left(\frac{z}{2z_d}\right), \qquad (6)$$

where m_d, R_d, and z_d denote the mass, radial scale-length, and vertical scale-height of the disk, respectively. Except for one model, we use $z_d = 0.15 R_d$ in all experiments, a choice which is consistent with observations of external galaxies (van der Kruit & Searle 1982; de Grijs & van der Kruit 1996). However, the observed scatter in z_d/R_d is quite substantial, reaching to values as small as 0.05. We show below that thinner disks lead to even stronger compression. Thus our assumption of $z_d = 0.15 R_d$ is conservative. We implicitly assume that the classical bulge is fully formed at the last major merger. Hernquist & Mihos (1995) showed that minor mergers drive gas to small radii leading to a burst of star formation and bulge growth. However dissipation is now thought to largely give rise to pseudo, not classical, bulges. The origin of bulges in high mass galaxies remains contentious. Weinzirl et al. (2009) used bulge+disk+bar decompositions to argue that mergers cannot account for the majority of bulges in current high mass galaxies. Hopkins et al. (2010) instead argued that major mergers dominate the formation of these bulges, with minor mergers contributing another $\sim 30\%$. Nonetheless a separation between classical and pseudo bulges seems to be well established, with observational evidence indicating that properties such as morphologies, star formation rates and correlations with disk properties, including color, change across $n \simeq 2$ (Drory & Fisher 2007; Fisher & Drory 2008; Fisher et al. 2009; Fisher & Drory 2010).

Each growing-disk simulation is performed by growing linearly over time the mass of an initially massless Monte Carlo particle realization of the desired disk model: $m_d(t) = (t/\tau)M_d$. In all simulations, we set $M_d = 1.6 \times 10^{11} M_\odot$ and $\tau = 2$ Gyr. During the experiments the disks are held rigid with their particles fixed in place, while both the bulge and halo particles are live, allowing them to remain in equilibrium as the disk mass grows. Throughout the experiments, all other properties of the growing disks (e.g., scale-lengths, scale-heights) are kept constant. Additional details of this technique can be found in Debattista et al. (2008), Villalobos et al. (2010) and Kazantzidis et al. (2010). Our simulations do not include a SMBH since the sphere of influence of the SMBH that would correspond to the velocity dispersion of the initial bulge, $r_h = GM_\bullet/\sigma_e^2$ is only ~ 4 pc, which is considerably smaller than $R_{e,0}$.

The initial conditions of the two-component galaxy contain a total of 4.4 million particles (4×10^6 dark matter particles and 4×10^5 bulge particles). The disk is modeled with a further 4×10^5 particles. Particles are set up using a quiet start procedure (Sellwood 1983) that ensures that all components have zero net momentum. We set up particles in groups of four: the first particle has (x, y, z, v_x, v_y, v_z) while the rest have $(-x, -y, z, -v_x, -v_y, v_z)$, $(-y, x, -z, -v_y, v_x, -v_z)$ and $(y, -x, -z, v_y, -v_x, -v_z)$.

We run 5 simulations, with varying ratio of disk scale-length to initial bulge effective-radius: $R_d/R_{e,0} = 0.5, 1, 2, 5,$ and 10. We save outputs at 25 Myr intervals corresponding to increments $\delta M_d = 0.25 M_b$. Table 1 provides a summary of a representative subset of the outputs.

All numerical simulations are carried out with the parallel N-body code PKDGRAV (Stadel 2001). In all experiments, we set the base timestep $\Delta t = 1.25$ Myr with timesteps refined such that $\delta t = \Delta t/2^p < \eta(\epsilon/a)^{1/2}$, where ϵ is the softening and a is the acceleration at a particle's current position, with rung number p as large as 29 allowed. For all simulations we set $\eta = 0.02$ and use an opening angle of the treecode $\theta = 0.7$. In the $R_d/R_{e,0} = 1$ model, timesteps for particles get as small as 2^{-10} of the base timestep, (*i.e.* 1220 years).

D/B	$R_d/R_{e,0}$	R_d/R_e	σ_e [$\mathrm{km\,s^{-1}}$]	$\Gamma_\bullet$
0	-	-	115.3 ± 0.3	-
0.25	0.5	0.61	126.9 ± 0.7	1.5
0.5	0.5	0.70	137.7 ± 1.2	2.0
1	0.5	0.83	155.9 ± 0.9	3.3
5	0.5	1.33	229.4 ± 2.3	15.7
10	0.5	1.62	279.1 ± 3.4	34.4
15	0.5	1.82	316.7 ± 4.1	56.9
20	0.5	1.98	345.2 ± 3.8	80.4
0.25	1	1.12	119.8 ± 0.3	1.2
0.5	1	1.22	124.5 ± 0.3	1.4
1	1	1.37	134.4 ± 1.8	1.8
5	1	1.99	177.4 ± 3.2	5.6
10	1	2.38	207.6 ± 5.1	10.5
15	1	2.63	231.1 ± 6.8	16.2
20	1	2.83	251.7 ± 9.6	22.7
0.25	2	2.10	116.2 ± 0.3	1.0
0.5	2	2.20	117.8 ± 0.6	1.1
1	2	2.36	121.9 ± 1.4	1.2
5	2	3.07	142.8 ± 2.9	2.4
10	2	3.53	161.4 ± 4.6	3.8
15	2	3.84	174.9 ± 5.2	5.3
20	2	4.07	186.3 ± 4.9	6.8
0.25	5	5.05	114.3 ± 0.3	1.0
0.5	5	5.11	113.9 ± 0.8	1.0
1	5	5.24	115.4 ± 0.8	1.0
5	5	5.96	122.4 ± 0.5	1.3
10	5	6.45	128.6 ± 1.6	1.5
15	5	6.81	134.6 ± 1.6	1.9
20	5	7.11	138.8 ± 2.1	2.1
0.25	10	10.02	113.2 ± 0.4	0.9
0.5	10	10.04	113.4 ± 0.9	0.9
1	10	10.14	113.7 ± 0.5	0.9
5	10	10.68	116.9 ± 0.8	1.1
10	10	11.22	119.4 ± 0.8	1.2
15	10	11.56	122.2 ± 1.3	1.3
20	10	11.80	123.5 ± 1.3	1.3

TABLE 1
A REPRESENTATIVE SAMPLING OF THE RESULTS AT DIFFERENT TIMES (CORRESPONDING TO DIFFERENT D/B) OF THE SIMULATIONS PRESENTED IN THIS PAPER. THE FIRST TWO COLUMNS LIST THE 'INPUT' PARAMETERS, WHERE D/B IS THE DISK-TO-BULGE MASS RATIO AND $R_d/R_{e,0}$ IS THE RATIO OF DISK SCALE-LENGTH TO INITIAL BULGE EFFECTIVE RADIUS. THE LAST THREE COLUMNS LIST THE OUTPUT PARAMETERS OF THE SIMULATIONS. R_d/R_e IS THE RATIO OF DISK SCALE-LENGTH TO FINAL BULGE EFFECTIVE RADIUS, σ_e IS THE VELOCITY DISPERSION OF THE BULGE AND $\Gamma_\bullet$ IS THE RATIO OF FINAL TO INITIAL $M_\bullet$ ASSUMING THE SYSTEM STARTS AND ENDS ON THE SAME $M_\bullet - \sigma_e$ RELATION WITH SLOPE $\beta = 4$. BOTH R_d/R_e AND σ_e INCLUDE THE EFFECTS OF RELAXATION OF THE INITIAL CONDITIONS. THE FIRST ROW CORRESPONDS TO THE INITIAL CONDITIONS BEFORE THE DISK IS GROWN.

3. EVOLUTION OF VELOCITY DISPERSION

Growth of the disk compresses the bulge and raises its velocity dispersion everywhere. In Figure 1 we plot examples of this evolution. From an initial value of

$\sim 100 \, \mathrm{km\,s^{-1}}$, the bulge in the $R_{\rm d}/R_{\rm e,0} = 1$ case attains values of $\sigma_r \sim 300 \, \mathrm{km\,s^{-1}}$. At each output we measure the bulge effective radius, $R_{\rm e}$, by computing the circular projected radius containing 50% of the bulge mass at inclinations $i = 0°, 60°$ and $90°$. A detailed analysis of the evolution of the structural parameters will be presented elsewhere. We then measured σ_e in slits as the root-mean-square (rms) of the line-of-sight velocity of all particles within R_e

$$\sigma_e{}^2 = \frac{\sum_{i \in R_e} m_i v_{i,los}^2}{\sum_{i \in R_e} m_i} = \frac{\int_0^{R_e} I(R)(\bar{v}_{los}^2 + \sigma_{los}^2)dR}{\int_0^{R_e} I(R)dR}, \quad (7)$$

where $\bar{v}_{los}$ is the mean line-of-sight velocity and σ_{los} is the line-of-sight velocity dispersion *along the slit*, which is placed along the major (*i.e.* inclination) axis. We repeat the measurements of σ_e for the same set of inclinations ($i = 0°$, $60°$ and $90°$) and use the average of these measurements for σ_e. Because σ_e is not identical for all viewing orientations, we use the largest difference between the average σ_e and the individual values as an estimate of the uncertainty on σ_e. We use slits of width 20 pc, which is $\simeq 4\%$ of $R_{\rm e,0}$ and $\simeq 16\%$ of the smallest $R_{\rm e}$ attained by the simulations, $\sim 0.14 \, \mathrm{kpc}$. The change in σ_e is not a result of different radial sampling caused by the change in $R_{\rm e}$, but is genuinely caused by evolution of the velocity dispersion, as can be seen in Figure 1. We also measure σ_8, the velocity dispersion in apertures of $R_{\rm e}/8$, similarly by restricting the sum in Eqn. 7 to that smaller radius.
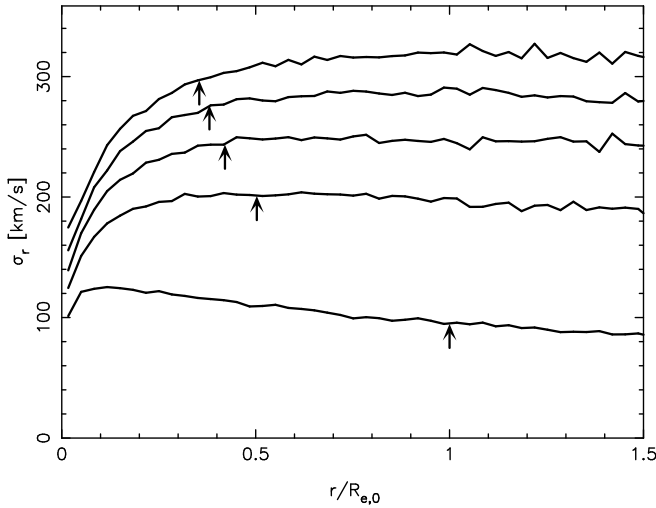

FIG. 1.— Evolution of σ_r, the radial component of the velocity dispersion in spherical coordinates, for the bulge particles in the $R_{\rm d}/R_{\rm e,0} = 1$ case. The profiles are at $D/B = 0, 5, 10, 15$ and 20, in increasing order. The arrows indicate $R_{\rm e}$ in each case.

The main simulation results are presented in Table 1 and plotted in Figure 2. In order to provide a fitting formula to these values, we note that Wolf et al. (2010) find $M_{1/2} \simeq 4G^{-1}R_{\rm e}\left\langle \sigma_{los}{}^2\right\rangle$ for pressure-supported systems, where $M_{1/2}$ is the mass within the half-mass radius and $\left\langle \sigma_{los}{}^2\right\rangle$ is the luminosity-weighted square of the line-of-sight velocity dispersion over the entire system.

We therefore expect σ to scale as

$$\left(\frac{\sigma_{los,f}(R_f)}{\sigma_{los,0}(R_0)}\right)^2 = \left(\frac{M_{b,f}(R_f) + M_d(R_f)}{M_{b,0}(R_0)}\right)\left(\frac{R_0}{R_f}\right) \quad (8)$$

where subscripts f and 0 indicate final and initial values and $M_b(R)$ and $M_d(R)$ indicate bulge and disk masses within radius R. Integrating over radius, we expect

$$\frac{\sigma_e}{\sigma_{e,0}} = \left(1 + 2\gamma\left[1 - \left(1 + \frac{R_{\rm e}}{R_{\rm d}}\right)e^{-R_{\rm e}/R_{\rm d}}\right]\frac{D}{B}\right)^{\delta}$$
$$\equiv \mathcal{F} \quad (9)$$

where $\sigma_{e,0}$ is the initial dispersion of the bulge. We stress that $\mathcal{F}$ is defined to be a *photometric*, not kinematic, quantity. Note that at fixed disk-to-bulge mass ratio, D/B, the minimum in $\mathcal{F}$ occurs at $R_{\rm e}/R_{\rm d} = 0$, *i.e.* as $R_{\rm d} \to \infty$. In deriving Eqn. 9 from the more general Eqn. 8 we have assumed that the disk is exponential; this is true for our simulations, but need not be the case in nature (e.g. Böker et al. 2003; Dutton 2009). If $\gamma = 1$ then the term in the outer brackets on the right hand side of Eqn. 9 is merely the ratio of final (bulge+disk) mass to initial (bulge only) mass within $R_{\rm e}$. (We ignore the dark matter halo in this calculation since the dark-to-bulge mass fraction within $R_{\rm e,0}$ is less than 2%.) We have also assumed that the disk scale-height is small compared to the effective radius of the bulge, but the factor γ is introduced to account for some of deviations resulting from this assumption. We have neglected the compression of the bulge in deriving this expression, *i.e.* we assume that $R_{\rm e} = R_{\rm e,0}$, which Table 1 clearly shows is not the case. We fold the uncertainty resulting from this assumption into the free parameter δ, which would be 0.5 if $R_{\rm e} = R_{\rm e,0}$. The best fit for $2 \leq R_{\rm d}/R_{\rm e} \leq 9$, $D/B > 0$ and $1 \leq \sigma_e/\sigma_{e,0} \leq 2$ is $\gamma = 0.3$ and $\delta = 1.76$ which gives a $\chi^2 = 172$ for 196 data points. The best fit value with $\gamma = 1$ is $\delta = 0.64$ with $\chi^2 = 562$. Likewise, we fitted best-fit parameters for σ_8 obtaining $\gamma = 0.02$ and $\delta = 15.92$ with a $\chi^2 = 719$. These best fits are shown in Figure 2. Because the compression of the bulge depends only on the ratios of bulge-to-disk masses and sizes, Eqn. 9 remains true for any galaxy or bulge mass, *i.e.* for any $\sigma_{e,0}$.

In order to check whether the bulge and halo respond adiabatically to the growth of the disk we slowly evaporated the disk from the final state of the simulation with $R_{\rm d}/R_{\rm e,0} = 1$. The results of this test are shown in Figure 3 and indicate that indeed the response is adiabatic to good approximation.

3.1. *Other dependencies and sources of scatter*

Eqn. 9 allows us to estimate the increase in σ_e for a bulge given a galaxy's photometric decomposition. We now explore the amount of scatter that can occur in these estimates for a given observed density distribution. Some of the effects we consider here will compress the bulge to a different extent, so both σ_e and $R_{\rm e}$ will change; it may happen however that Eqn. 9 still provides a good approximation to the evolution of σ_e. Because we use Eqn. 9 to estimate the offset of galaxies from the $M_{\bullet} - \sigma_e$ relation, we are primarily interested in those changes which Eqn. 9 does *not* reproduce, and we consider this to be the scatter of interest here.
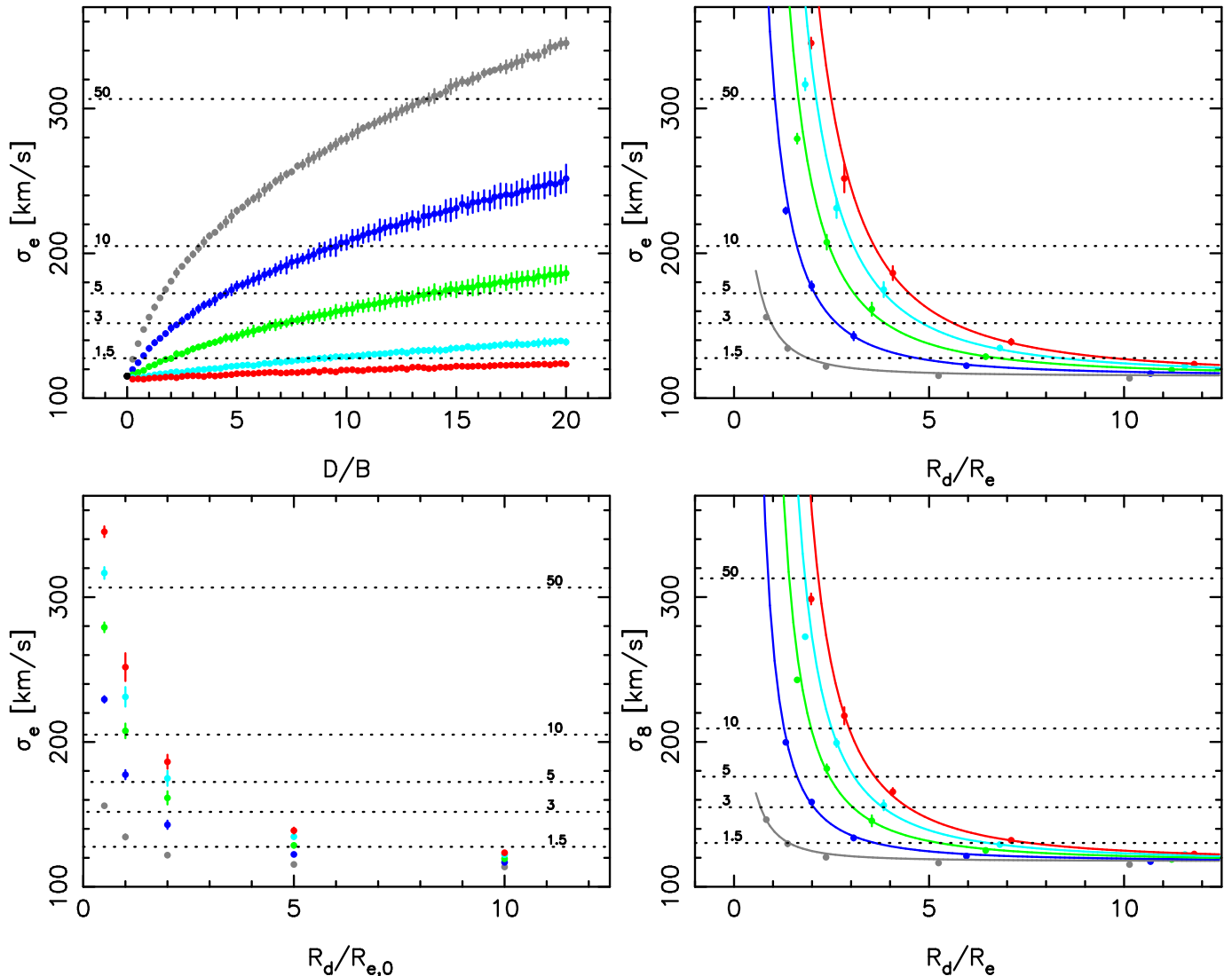
FIG. 2.— **Left**: σ_e as a function of D/B (top) and $R_{\rm d}/R_{\rm e,0}$ (bottom). Gray, blue, green, cyan and red represent, respectively, $R_{\rm d}/R_{\rm e,0}$ = 0.5, 1, 2, 5 and 10 in the top panel and D/B = 1, 5, 10, 15 and 20 in the bottom panel. The initial conditions are indicated by the black point in the top panel. **Right**: σ_e (top) and σ_8 (bottom) as functions of $R_{\rm d}/R_{\rm e}$. Colors are as in the bottom-left panel. The solid lines show our fitting function, Eqn. 9. In each panel, the dotted horizontal lines show contours of constant $(\sigma/\sigma_0)^4$, with values indicated above each contour.

The (re)-assembly of disk galaxies is not necessarily a slow, adiabatic process. A possible source of scatter might therefore be due to disks growing more rapidly than assumed here. In order to test what the effect of faster disk growth may be, we grow the disk ten times faster, *i.e.* within 200 Myr. The results are shown in the top panel of Figure 4. The effect of the different growth rate is negligible.

At a given mass, the concentration of dark matter halos can vary substantially (e.g. Wechsler et al. 2002). We explore what effect this might have on σ_e by re-running our simulation with a halo having $c = 20$. The bottom panel of Figure 4 shows that σ_e is barely changed, undoubtedly because the galaxy is baryon-dominated in the bulge region. Reasonable variations in halo concentration therefore do not produce any significant scatter in the $M_\bullet - \sigma_e$ relation.

All simulations above used $z_{\rm d} = 0.15R_{\rm d}$. In the top panel of Figure 5 we show the effect of halving $z_{\rm d}$. This increases the final σ_e to $268.7 \pm 13.3 {\rm km\,s}^{-1}$, an increase by

6.8% while $R_{\rm e}$ decreases by $\sim 3.3\%$. The bottom panel of Figure 5 shows that, taken together, these differences lower the quality of the fit of Eqn. 9 for $z_{\rm d} = 0.075R_{\rm d}$ compared with that for the standard $z_{\rm d} = 0.15R_{\rm d}$, although all cases still have errors of less than 15%. At $\sigma_e/\sigma_{e,0} = 1.8$ the *maximum* error is about 12%, which we adopt as our estimate for the scatter due to disk thickness.

Another source of scatter comes from the contamination of measured bulge kinematics by the kinematics of the disk, which is almost inevitable in real galaxies. Exploring this effect requires that we set up equilibrium kinematics for the disks in the $R_{\rm d}/R_{\rm e,0} = 1$ model at various values of D/B. We set the kinematics of the disks to give constant Toomre-$Q = 1.5$, as described in Debattista & Sellwood (2000). For this we calculate the potential using a hybrid polar-grid code with the disk on a cylindrical grid and the bulge+halo on a spherical grid (Sellwood 2003). Figure 6 shows the effect of disk contamination: changes in σ_e can be either positive or neg-
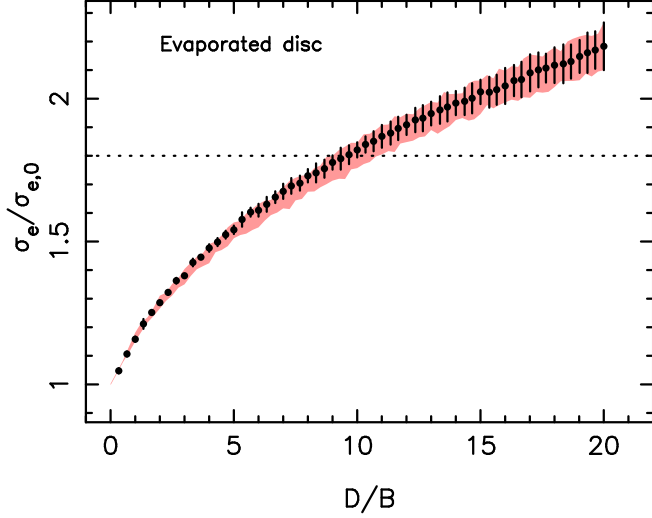
FIG. 3.— Evolution of σ_e in the $R_d/R_{e,0} = 1$ model as the disk is grown (red shaded region) and subsequently evaporated (black points with error bars). The dotted horizontal line indicates $\sigma_e/\sigma_{e,0} = 1.8$ for which $\Gamma_\bullet = 10.5$ if $\beta = 4$.
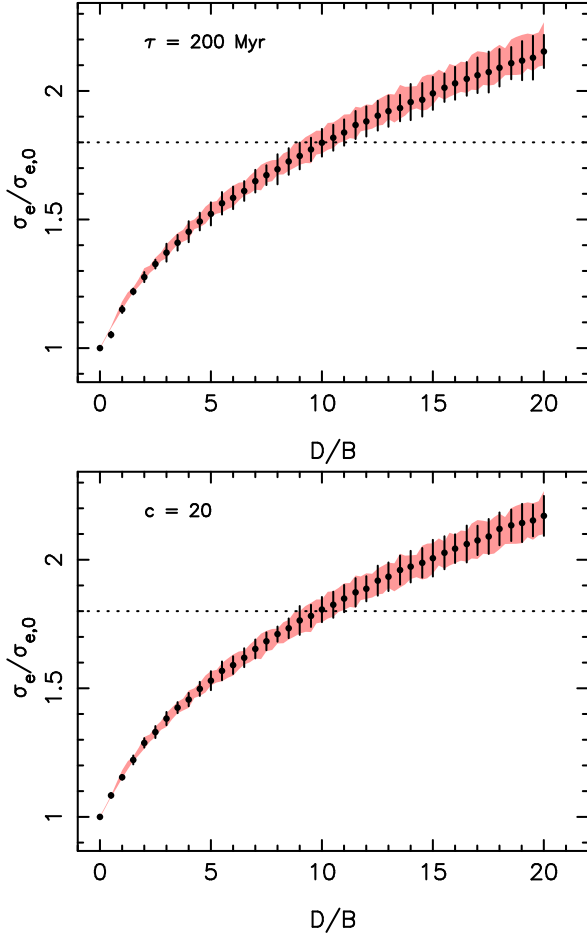

FIG. 4.— Evolution of σ_e in the $R_d/R_{e,0} = 1$ model for different variations from our fiducial simulation. In both panels the shaded red region represents the evolution in the fiducial case, while the black points with error bars show the variant simulation results. The dotted horizontal lines indicate $\sigma_e/\sigma_{e,0} = 1.8$ for which $\Gamma_\bullet = 10.5$. Top: Effect of growing the disk in 200 Myr instead of 2 Gyr. Bottom: Effect of the halo having concentration $c = 20$ instead of $c = 10$.
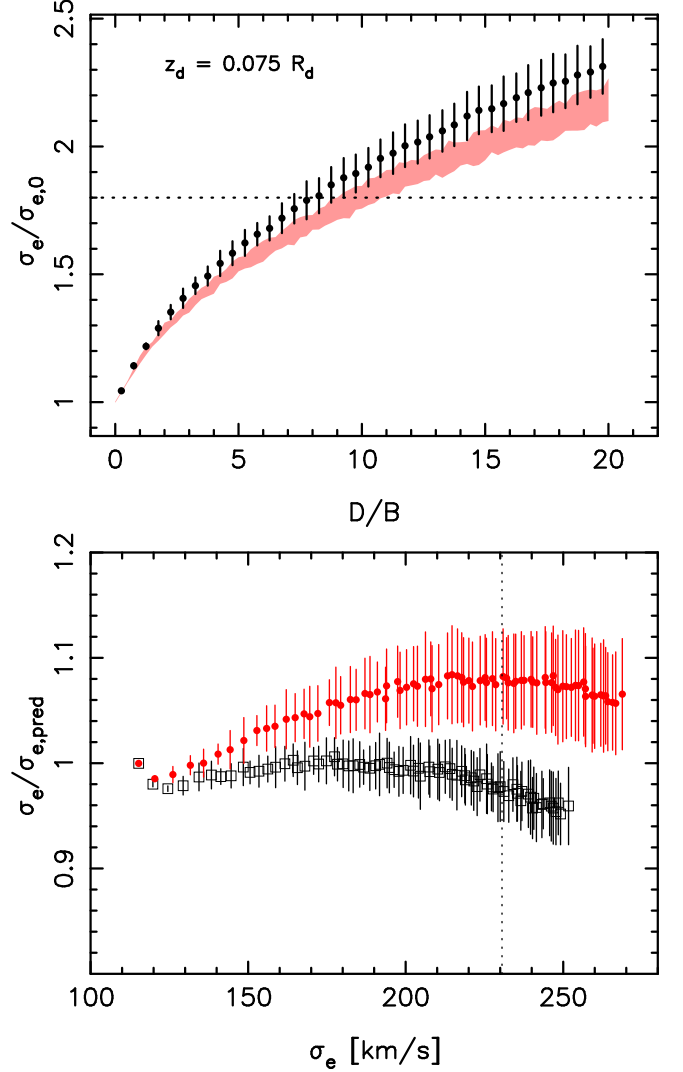
FIG. 5.— Comparision of the evolution of σ_e in the $R_d/R_{e,0} = 1$ model with a thinner disc $z_d = 0.075R_d$ instead of the fiducial $z_d = 0.15R_d$. Top: The shaded red region represents the evolution in the fiducial case, while the black points with error bars show the thinner disk. The dotted horizontal line indicates $\sigma_e/\sigma_{e,0} = 1.8$ for which $\Gamma_\bullet = 10.5$. Bottom: A comparison of the fit of Eqn. 9 for the fiducial case (black open squares) and with $z_d = 0.075R_d$ (red filled circles). The dotted vertical line indicates $\sigma_e/\sigma_{e,0} = 1.8$.

ative, but generally $|\sigma_e(B) - \sigma_e(B + D)|/\sigma_e(B) \lesssim 25\%$. The error increases with σ_e, which is a result of the increasing D/B. An independent analysis of the effect of disk contamination on σ_e by Hartmann et al. (*in preparation*) also finds fractional changes $\lesssim 25\%$. The open stars in Figure 6 show the inclination-averaged values of $\sigma_e(B)$ versus $\sigma_e(B + D)$; the differences between the means are generally less than 20%. However on average $\sigma_e(B + D)$ is systematically larger than $\sigma_e(B)$.

Based on these tests we conclude that there is $\lesssim 30\%$ uncertainty in the degree to which classical bulges are compressed.

3.2. *Observational evidence for bulge compression*

We now present evidence that bulge compression associated with disk regrowth has occurred in nature by comparing the properties of classical bulges and elliptical galaxies. This requires a large sample of disk galax-
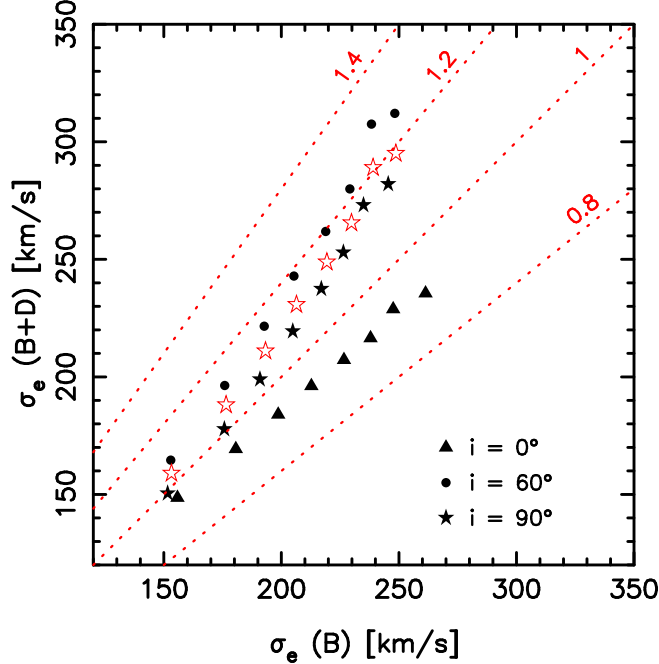
FIG. 6.— The effect of including disk stars in the measurement of σ_e. $\sigma_e(B)$ represents the measurement from bulge particles only while $\sigma_e(B+D)$ includes disk particles in the measurement. Dotted lines have constant slope, as indicated along each line. The different points represent the effect of disk contamination as D/B increases from 2.5 to 20. Different filled symbols correspond to different galaxy inclinations, as indicated. Open (red) stars correspond to inclination-averaged values.

FIG. 7.— Distributions of ellipticals and classical bulges, taken from Gadotti (2009) and Gadotti & Kauffmann (2009), in the σ_8-M_{bul} plane. Left: Elliptical galaxies. Center: Classical bulges in unbarred galaxies. Right: The same sample as in the central panel, but using the decompressed values for σ_8 obtained by applying Eqn. 9. The (red) solid lines in each of the upper panels show the best fit to the elliptical galaxies. The bottom panels show the residuals for each sample from this best fit to the ellipticals: $\Delta \log \sigma_8 = \log \sigma_8 - \log \sigma_{8,\mathrm{fit}}$, where $\sigma_{8,\mathrm{fit}}$ is the σ_8 value from the fit to the ellipticals of a given mass.

ies with bulge+disk decompositions. Gadotti (2009) presented a detailed structural analysis of nearly 1000 galaxies from the Sloan Digital Sky Survey (SDSS) (York et al. 2000), classifying them into ellipticals or disks, distinguishing the latter by whether they host classical or pseudo bulges. Gadotti & Kauffmann (2009) present the velocity dispersions within $R_e/8$, hereafter σ_8, for a fraction of these galaxies. We use these data to compare the distributions of σ_8 for ellipticals and classical bulges. The sample contains 196 elliptical galaxies and 176 unbarred classical bulges with kinematic data. Gadotti (2009) classifies the bulges based on the Kormendy (mean effective surface brightness $\langle \mu_e \rangle$ versus R_e) relation (Kormendy 1977). Fisher & Drory (2008) identify Sérsic index $n = 2$ as the dividing line between pseudo and classical bulges, with the latter having $n > 2$. We apply this additional criterion to the sample, which leaves 166 galaxies as our final sample of unbarred, classical bulges.

Figure 7 plots the distribution of galaxies in the σ_8-M_{bul} plane for ellipticals, observed unbarred classical bulges, and the same classical bulges if they are decompressed using Eqn. 9. We obtain M_{bul}, D/B and R_e/R_d from the the exponential disk+ Sérsic bulge decompositions of Gadotti (2009) and σ_8 from Gadotti & Kauffmann (2009). We decompress to obtain $\sigma_{8,0}$ using Eqn. 9 fitted to σ_8.

The line in the top panels of Figure 7 shows the fit to the ellipticals: $\sigma_8/\mathrm{km\,s^{-1}} = (M_{bul}/3051 M_\odot)^{0.30783}$. The observed classical bulges have larger σ_8, on average, than the ellipticals at a given M_{bul}. When we decompress the bulges their offset from the elliptical relation is significantly reduced, as can be seen in the bottom panels of Figure 7. The distributions of the residuals from
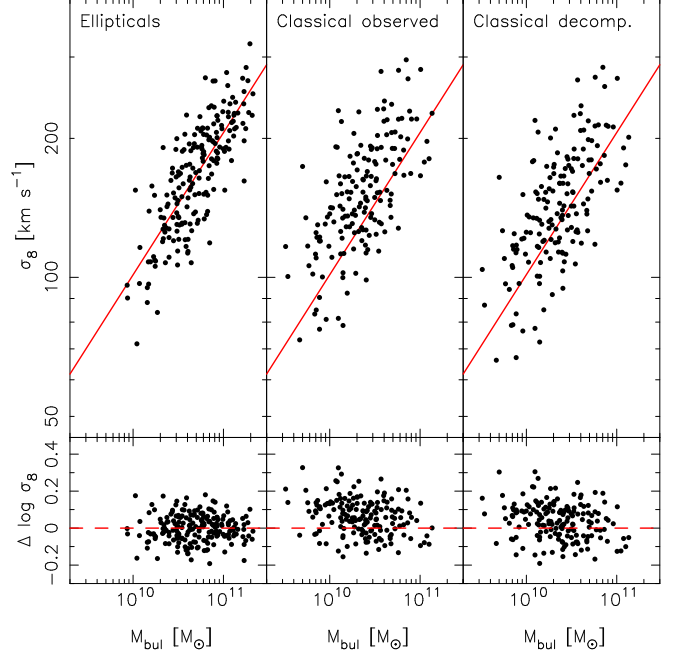
the fit to ellipticals are shown in Figure 8. The means of the residuals are 0.06 dex and 0.04 dex for the observed and decompressed classical bulges, respectively. A two-sample unbinned K-S test comparing the ellipticals and bulges shows that the probability that the residuals are drawn from the same distribution is 3×10^{-9} for the observed bulges and a much larger, though still formally small, 3×10^{-6} for the decompressed bulges. In Figure 9 we plot the distribution of the bulges and ellipticals in the σ_8-R_e plane. As was also found by Gadotti (2009), the observed classical bulges are offset to larger σ_8 and smaller R_e relative to the ellipticals in this projection of the Fundamental Plane, as expected if bulges are compressed by disks.

While Figures 7 and 8 do provide evidence for bulge compression, they also show that the σ_8 is even larger than predicted by our simple model. Possibly this is because disks are more concentrated than exponential at the center, as proposed by Böker et al. (2003) and Dutton (2009). Alternatively, contamination of σ_8 by the disk, or differences in formation histories, could be to blame for (part of) the offset between ellipticals and classical bulges. We note that if disks are more concentrated than exponential then their effect is to further compress bulges and we have under-estimated the evolution of σ_e. Exploration of this issue is deferred to a future publication.

4. CONSEQUENCES FOR THE $M_\bullet - \sigma_e$ RELATION

The steepness of the $M_\bullet - \sigma_e$ relation implies that the maximum factor of ~ 3 increase in σ_e obtained in the simulations would require a factor of ~ 80 increase in
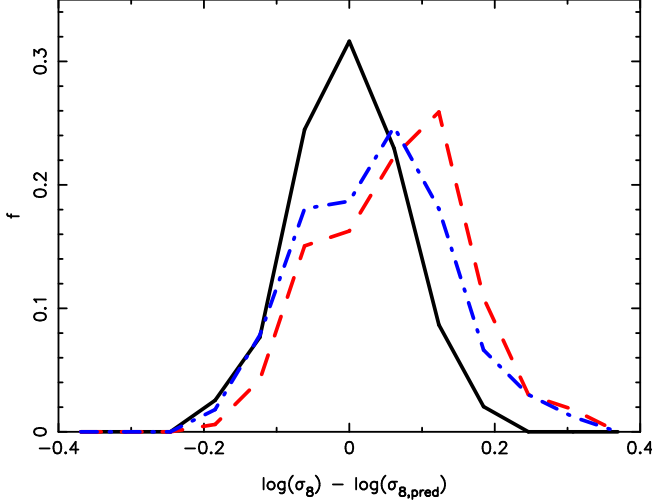
FIG. 8.— Distributions of the residuals shown in the lower panels of Fig. 7. The solid (black) line is for the ellipticals, the dashed (red) line is for observed classical bulges (as described in the text) and the dot-dashed (blue) line is for the classical bulges decompressed using Eqn. 9.
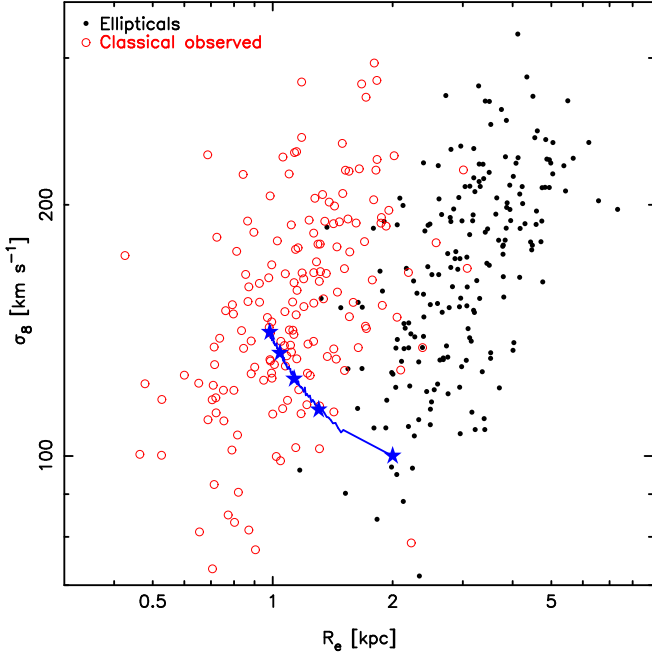

FIG. 9.— The σ_8-R_e projection of the fundamental plane for the Gadotti & Kauffmann (2009) sample. The (black) filled circles show elliptical galaxies while the (red) open circles show the observed unbarred classical bulges. The diagonal (blue) line shows the evolution of the model in the simulation with $R_d/R_{e,0} = 2$, assuming $R_{e,0} = 2$ kpc and $\sigma_{e,0} = 100 \, \mathrm{km \, s^{-1}}$. The star symbols correspond to the system at D/B = 0 (bottom right), 5, 10, 15 and 20 (top left).

$M_\bullet$ for the SMBH to remain on the relation, more than $6\times$ larger than the factor of 20 by which the stellar mass grew. We define the factor by which $M_\bullet$ must grow to remain on the $M_\bullet - \sigma_e$ relation, $\Gamma_\bullet \equiv M_{\bullet,f}/M_{\bullet,0} = (\sigma_e/\sigma_{e,0})^\beta$, where subscripts 0 and f indicate initial and final values. The dotted contours in Figure 2 indicate $\Gamma_\bullet$ assuming $\beta = 4$. Values of $\Gamma_\bullet$ for the simulations are listed in Table 1. In general $\Gamma_\bullet > 3$ requires that $R_d/R_e \lesssim 5$ and D/B $\gtrsim 2$.
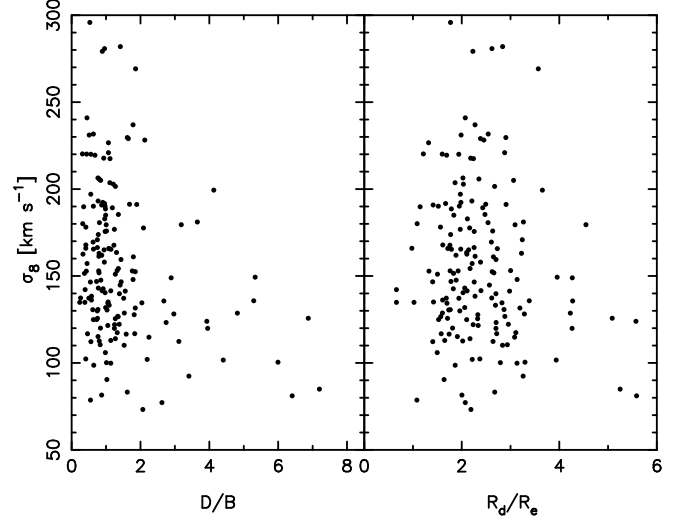

FIG. 10.— Dependence of σ_8 on the parameters of bulge+disc decompositions for unbarred classical bulges in the sample of Gadotti (2009).

4.1. Evolution of slope and zero-point

In Figure 10 we plot the distribution of σ_8 as a function of D/B and of R_d/R_e for the Gadotti (2009) sample; a weak correlation between D/B and σ_8 is present (Spearman $r_{sp} = -0.22$, Kendall $\tau = -0.15$), which is statistically significant at less than 3σ. The correlation between R_d/R_e and σ_8 is even weaker (Spearman $r_{sp} = -0.10$, Kendall $\tau = -0.07$). We therefore neglect these weak correlations. If $\sigma_e/\sigma_{e,0} = \mathcal{F}$, and the average $\sigma_e/\sigma_{e,0}$ at a given $\sigma_{e,0}$ is $\langle \mathcal{F} \rangle$, then neglecting these correlations implies that $\langle \mathcal{F} \rangle$ is independent of $\sigma_{e,0}$. Then we can write the $M_\bullet - \sigma_e$ relation for compressed bulges, if $M_\bullet$ does not change while disks grow, as

$$\log M_\bullet = \alpha - \beta \log \langle \mathcal{F} \rangle + \beta \log \sigma_e \qquad (10)$$

i.e. the slope of the relation remains β but the zero-point changes by

$$\delta \alpha = -\beta \log \langle \mathcal{F} \rangle . \qquad (11)$$

Because $\mathcal{F} \geq 1$ (compression can only increase σ_e) Eqn. 11 implies that $\delta \alpha < 0$. Therefore, if $M_\bullet$ does not grow during disk formation, the $M_\bullet - \sigma_e$ relation of compressed bulges will be parallel to, but offset below, the $M_\bullet - \sigma_e$ relation for elliptical galaxies. Failure to find such an offset would strongly suggest that SMBHs grow along with disks.

4.2. Predicted offset from photometric samples

In order to provide a quantitative prediction for the change in the zero-point we use two samples of galaxies with detailed photometric decompositions. The first is the sample of Gadotti (2009), for which each galaxy is fit with three components; a bulge, a disk, and, where necessary, a bar. We split the sample by whether the galaxy is barred or not. In our analysis, for the barred galaxies we treat the bar as part of the disk when computing D/B values and use R_d from the disk, not the bar. Because bars are at the centers of galaxies, our assumption underestimates the fraction of disk+bar mass within the bulge effective radius, and therefore also $\langle \mathcal{F} \rangle$. The second sample is the complete and volume-limited catalogue of 86 low-inclination disk galaxies of all Hubble types observed
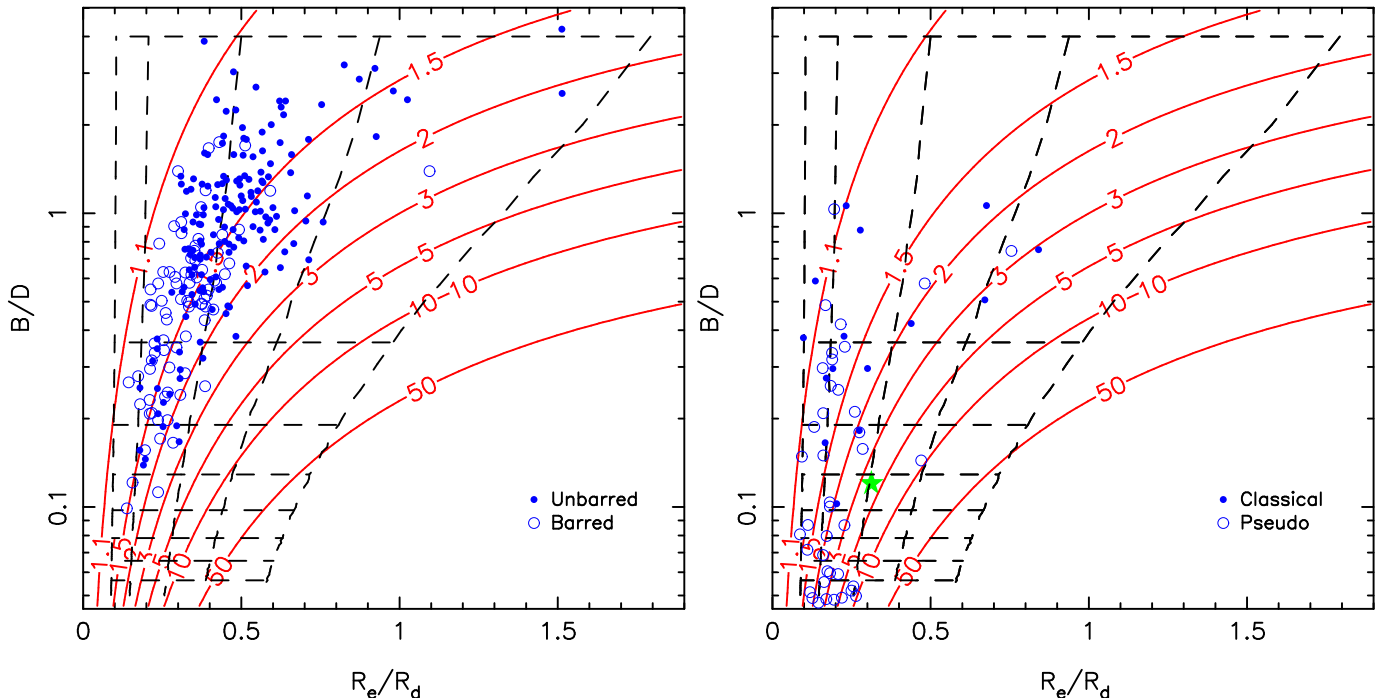
FIG. 11.— Contours of predicted $\Gamma_\bullet$ in the B/D-R_e/R_d plane assuming the Gültekin et al. (2009) value of $\beta = 4.24$ (solid lines). The dashed lines correspond to our simulation grid, with horizontal lines at fixed D/B and roughly vertical lines at constant $R_d/R_{e,0}$. A galaxy growing a disk at fixed R_d evolves from top to bottom parallel to the dashed lines. Left: The (blue) circles are data from Gadotti (2009), with open and filled circles corresponding to barred and unbarred galaxies, respectively. See text for details of how the parameters for the barred galaxies are computed. Right: The (blue) circles are data from Graham (2003), with open and filled circles corresponding to galaxies with $n < 2$ (pseudo) bulges and $n > 2$ (classical) bulges, respectively. The (green) star represents the Milky Way based on the model of Bissantz & Gerhard (2002).

by de Jong & van der Kruit (1994). For 75 of these, Graham (2003) fitted Sérsic bulge+exponential disk decompositions in the K-band, regardless of whether they are barred or not. We select classical bulges from this sample as those galaxies having $n > 2$, leaving us with 15 galaxies.

Figure 11 plots the distribution of both samples in the R_d/R_e-D/B plane and overlays contours of $\Gamma_\bullet$. All but one of the classical bulges in both samples have D/B < 10, whereas many of the pseudo bulges in the Graham (2003) sample have D/B > 10. The majority of the galaxies in the Gadotti (2009) sample cluster in the range $0.2 \lesssim R_e/R_d \leq 0.6$ ($1.6 \leq R_d/R_e \lesssim 5$). For about half of all galaxies $\Gamma_\bullet > 1.4$, while a small fraction ($\sim 33\%$ of the Graham (2003) sample and $\sim 8\%$ in the Gadotti (2009) sample) has $\Gamma_\bullet > 2$. A small number of galaxies fall outside the simulation grid. In calculating $\Gamma_\bullet$ for these galaxies, we extrapolate Eqn. 9 to outside our simulation grid. These are mostly however at large D/B, and populated solely by pseudo bulges, rather than classical ones. Many more galaxies in the Gadotti (2009) sample have D/B < 1 than in the Graham (2003) sample. The difference cannot be attributed to the different photometric decompositions since the same difference is present also for unbarred galaxies in the Gadotti (2009) sample. Therefore together these two samples should give some indication of the uncertainty in the photometric parameter $\langle \mathcal{F} \rangle$. The distributions of $\mathcal{F}$ for both samples are shown in Figure 12 and the results listed in Table 2. Notwithstanding the differences between the samples, we find a narrow range of $1.096 \leq \langle \mathcal{F} \rangle \leq 1.122$. Assuming $\beta = 4.24$ (Gültekin et al. 2009), this corre-

sponds to $1.48 \leq \langle \Gamma_\bullet \rangle \leq 1.63$ and $-0.21 \leq \delta\alpha \leq -0.17$. For their full sample Gültekin et al. (2009) measured $\alpha = 8.12 \pm 0.08$; with such a small uncertainty on α, offsets between classical bulges and elliptical galaxies in the $M_\bullet - \sigma_e$ relation should be measureable. We estimated above a scatter due to modelling uncertainties of order 30%, but the effect we are looking for here is systematic, so it should be detectable if present.

Sample	N_g	$\langle \mathcal{F} \rangle$
Unbarred Gadotti (2009)	166	1.098 ± 0.004
Barred Gadotti (2009)	80	1.096 ± 0.005
All Gadotti (2009)	246	1.098 ± 0.003
Classical Graham (2003)	15	1.122 ± 0.025

TABLE 2
VALUES OF $\langle \mathcal{F} \rangle$ FOR DIFFERENT PHOTOMETRIC SAMPLES. N_g INDICATES THE NUMBER OF GALAXIES IN EACH SAMPLE. THE ERROR ON $\langle \mathcal{F} \rangle$ IS PURELY STATISTICAL.

5. TESTING FOR OFFSETS

We now test for offsets between the $M_\bullet - \sigma_e$ relations of elliptical galaxies and of classical bulges. We show that there is no significant offset between the two populations. If we decompress the bulges using Eqn. 9 then a small but significant offset occurs, which supports our claim that an offset should have been detected if SMBHs had not grown in mass along with disks.
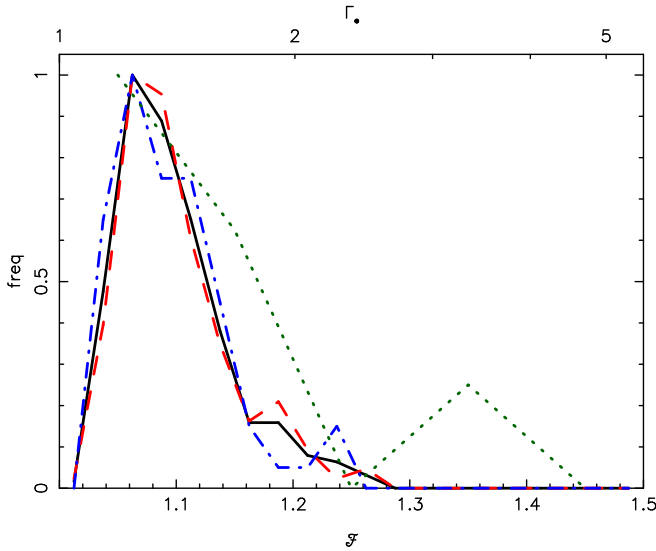
5.1. Gültekin sample

FIG. 12.— The distribution of $\mathcal{F}$ for the various photometric samples. The dotted (green) line shows the classical bulges in the Graham (2003) sample. The remaining lines are for the Gadotti (2009) sample of classical bulges: the dashed (red) line is for unbarred galaxies, dot-dashed (blue) line for barred galaxies and solid (black) line for all galaxies. For ease of comparison, all distributions have been normalized to unit peak value. The top border is labelled by $\Gamma_\bullet$ assuming $\beta = 4.24$ (Gültekin et al. 2009).

Gültekin et al. (2009) presented a sample of 49 galaxies with $M_\bullet$ measurements, to which they fitted the $M_\bullet - \sigma_e$ relation. Many of these galaxies have bulge+disk decompositions in the literature (Fisher & Drory 2008, 2010, 2011). The photometric decompositions we use here were taken from Fisher & Drory (2008), Fisher & Drory (2010) and Fisher & Drory (2011). For the unpublished decompositions the Appendix provides a description of how they were performed. The left panel of Figure 13 presents these photometric decompositions with contours of $\Gamma_\bullet$ from Eqn. 9 overlaid.

Gültekin et al. (2009) found $\alpha = 8.23$ for ellipticals and $\alpha = 8.17$ for classical bulges, but their definition of classical bulges includes the elliptical galaxies. We therefore refit the relation to ellipticals and classical bulges separately using the code MPFITEXY[6] which implements the MPFIT algorithm (Markwardt 2009). We first fit the $M_\bullet - \sigma_e$ relation of the elliptical galaxies in the Gültekin et al. (2009) sample: IC 1459, M32, M60, M84, M87, NGC 821, NGC 1399 (both measurements), NGC 2778, NGC 3377, NGC 3379, NGC 3607, NGC 3608, NGC 4261, NGC 4291, NGC 4459, NGC 4473, NGC 4486A, NGC 4697, NGC 5077, NGC 5576, NGC 5845, NGC 6251, NGC 7052, A1836 and A3565. We obtain $\beta = 4.06 \pm 0.40$, with zero-point $\alpha = 8.21 \pm 0.07$ and an intrinsic scatter of 0.30. This measurement is in excellent agreement with the $M_\bullet - \sigma_e$ relation of elliptical galaxies obtained by Gültekin et al. (2009) using a different fitting method. This $M_\bullet - \sigma_e$ relation is shown by the solid line in the right panel of Figure 13. We then selected the classical bulges to be those having $n > 2$, leaving us with 16 galaxies: NGC 224, NGC 1023, NGC 2787, NGC 3031, NGC 3115, NGC 3227, NGC 3245 NGC 3585, NGC 3998, NGC 4026, NGC 4258, NGC 4342, NGC 4564, NGC 4594, NGC 4596 and NGC 7457. For this sam-

[6] http://purl.org/mike/mpfitexy

ple we measure, from the photometric decompositions, $\langle \mathcal{F} \rangle = 1.12 \pm 0.03$, comparable to the values predicted in Table 2. Based on this value and fixing $\beta = 4.06$, we expect $\delta\alpha = -0.20$ if $M_\bullet$ had not changed as the disks grew. Fitting the $M_\bullet - \sigma_e$ relation for classical bulges while holding β fixed, we obtain $\alpha = 8.29 \pm 0.09$, which is plotted as the dashed line in Figure 13. The offset from the elliptical relation is only 0.08, within the one sigma uncertainty and significantly smaller than expected from the photometric decomposition if no SMBH growth had occurred. The zero-point predicted by the photometric decompositions is ~ 2 sigma away from the one found. Thus we find no evidence of a significant offset between elliptical galaxies and observed classical bulges.

In order to demonstrate that bulge compression should have produced an offset that is measureable, we also fitted the $M_\bullet - \sigma_e$ relation of the same bulges decompressed using Eqn. 9, again fixing $\beta = 4.06$ and using as uncertainties on $\sigma_{e,0}$ and $M_\bullet$ the values for the observed bulges. We obtain $\alpha = 8.47 \pm 0.11$. The offset from the relation for ellipticals is now $+0.26$, which is two sigma different. This fit is shown in the right panel of Figure 13 as the dot-dashed line.

5.2. *Beifiori sample*

As a further demonstration of the absence of an offset in the $M_\bullet - \sigma_e$ relation between ellipticals and classical bulges we consider also the independent sample of Beifiori et al. (2009). Beifiori et al. (2009) obtained upper limits on the masses of SMBHs in over 100 galaxies. They showed that their relation is parallel to the usual $M_\bullet - \sigma_e$ relation, with $\beta = 4.12 \pm 0.38$. For a number of these galaxies, Beifiori et al. (2012) provide bulge+disk decompositions; the resulting sample has 22 disk galaxies. Of these, 16 galaxies have $n > 2$ which we select as classical bulges: NGC 2911, NGC 2964, NGC 3627, NGC 3675, NGC 3992, NGC 4203, NGC 4245, NGC 4314, NGC 4429, NGC 4450, NGC 4477, NGC 4548, NGC 4579, NGC 4698, NGC 5005 and NGC 5252. The left panel of Figure 14 plots the distribution of these bulges in the B/D-R_e/R_d plane. From their photometric decompositions we obtain $\langle \mathcal{F} \rangle = 1.16 \pm 0.03$.

Because this sample only has upper limits on $M_\bullet$, not actual measurements, we fit the $M_\bullet - \sigma_e$ relation keeping the slope of the relation fixed to that obtained for the elliptical galaxies from the Gültekin et al. (2009) sample, *i.e.* $\beta = 4.06$. Although the Beifiori et al. (2009) sample of upper limits cannot give the absolute zero-point of the relation, we are interested in relative offsets, for which it is well suited. As an estimate for the error on $M_\bullet$ we use half the difference between the two upper limits given by Beifiori et al. (2009), which are based on assuming two different inclinations for the nuclear disk surrounding the SMBH. Using a constant error of $10^3 M_\odot$ instead yields results that are virtually indistinguishable. We fit the zero-points for ellipticals ($\alpha = 8.46 \pm 0.10$), observed classical bulges ($\alpha = 8.57 \pm 0.10$) and decompressed classical bulges ($\alpha = 8.95 \pm 0.11$). These results are shown in the right panel of Figure 14. The offset between the ellipticals and the observed classical bulges is 0.11, which is again less than one sigma. In comparison, the offset between ellipticals and decompressed classical bulges, shown in the right panel of Figure 13, is $+0.49$ (the photometric prediction being $\delta\alpha = 0.26$), which is different
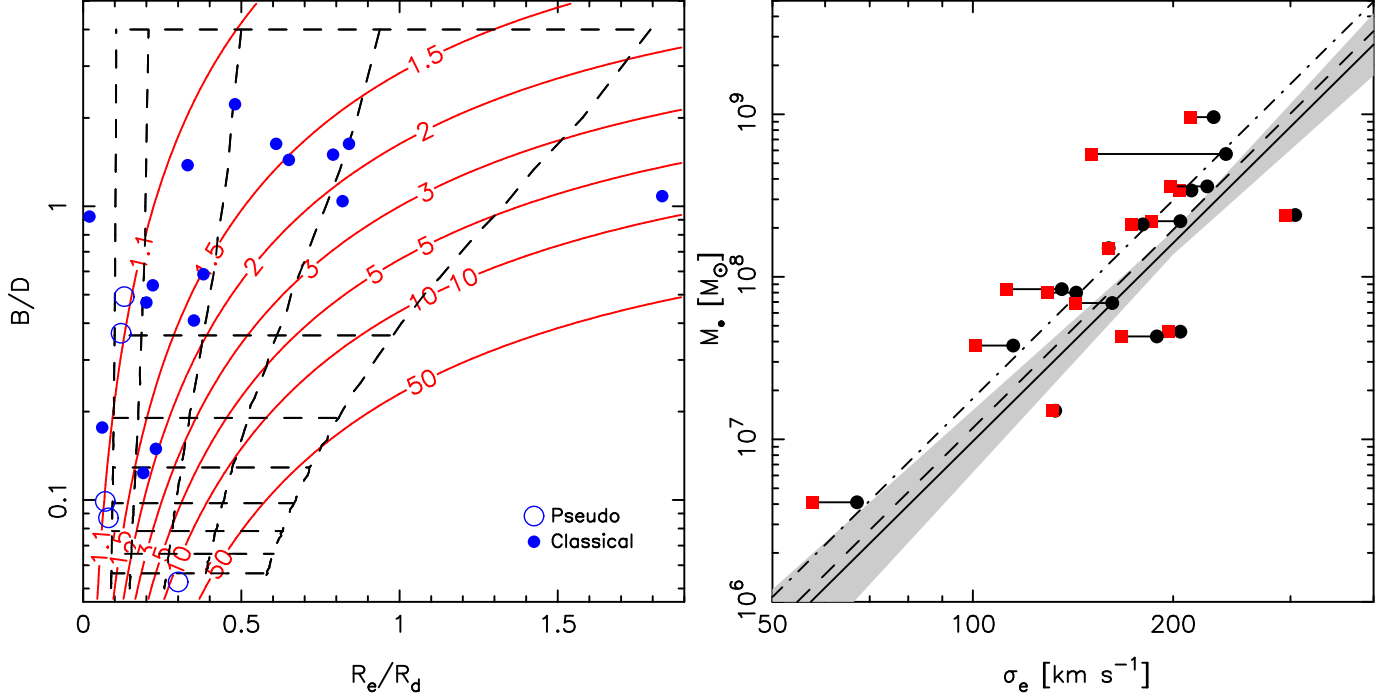
FIG. 13.— The sample of Gültekin et al. (2009) with bulge+disk fits as described in the text. Left panel: Distribution of the sample in the B/D-R_e/R_d plane. Filled symbols show $n > 2$ (classical) bulges while open symbols show $n < 2$ (pseudo) bulges. Contours of $\Gamma_\bullet$ assume $\beta = 4.24$, as before. Right panel: The $M_\bullet - \sigma_e$ relation for the 16 classical bulges. The (black) circles with larger values mark the observed σ_e while the connected (red) squares show $\sigma_{e,0}$ (i.e., the decompressed values) from the fit of Eqn. 9. The solid line shows our re-fit for the $M_\bullet - \sigma_e$ relation of elliptical galaxies ($\alpha = 8.21$, $\beta = 4.06$) while the dashed and dot-dashed lines show the observed ($\alpha = 8.29 \pm 0.09$) and decompressed ($\alpha = 8.47 \pm 0.11$) classical bulges fitted by a relation with $\beta = 4.06$. The shaded region shows the one sigma uncertainty on the $M_\bullet - \sigma_e$ relation of ellipticals.

at more than three sigma. Hence, for this sample the observed offset and the offset predicted if no SMBH growth occurs differ by > 3 sigma.

Thus both the Gültekin et al. (2009) sample, with full $M_\bullet$ measurements, and the Beifiori et al. (2009) sample with $M_\bullet$ upper limits only, show no evidence for an offset between the $M_\bullet - \sigma_e$ relation of ellipticals and of classical bulges, even though the disks should have compressed the bulges to a measureable extent. We therefore conclude that SMBHs in classical bulges have been growing along with disks.

5.3. Galaxies with $\Gamma_\bullet > 3$

We estimated above that the scatter in $\sigma_e/\sigma_{e,0}$ is $\lesssim 30\%$. This implies that galaxies in which $\mathcal{F} > 1.3$, (i.e. $\Gamma_\bullet > 2.9$ for $\beta = 4$) should be dominated by compression. Table 3 lists the five galaxies for which the photometric properties imply $\Gamma_\bullet \geq 3$; these are the galaxies for which the impact of compression is the largest, and are therefore ideally suited to test whether or not disk (re-)assembly is associated with growth of the SMBH. Of the five galaxies, only one, NGC 4594 (the Sombrero galaxy), which happens to have the largest $\Gamma_\bullet$, has a proper $M_\bullet$ mass measurement. Two of the other galaxies have $M_\bullet$ upper limits from Beifiori et al. (2009). The remaining two galaxies have no $M_\bullet$ measurements that we are aware of. We recommend measurements of $M_\bullet$ in these galaxies in order to further constrain the ability of SMBHs to grow along with disks.

Figure 15 plots the ratio of the observed $M_\bullet$ to that predicted for its value of σ_e by the $M_\bullet - \sigma_e$ relation of ellipticals versus $\Gamma_{\bullet,\mathrm{phot}} \equiv \mathcal{F}^\beta$, the value of $\Gamma_\bullet$ predicted

Galaxy	$\Gamma_\bullet$	Reference
NGC 4594	6.6	Fisher & Drory (2011)
NGC 3675	4.1	Beifiori et al. (2012)
NGC 438	3.1	Graham (2003)
NGC 3627	3.0	Beifiori et al. (2012)
NGC 3140	3.0	Graham (2003)

TABLE 3
GALAXIES FOR WHICH THE PHOTOMETRIC DATA PREDICTS $\Gamma_\bullet \geq 3$ ASSUMING THE $M_\bullet - \sigma_e$ RELATION OF ELLIPTICALS $((\alpha, \beta) = (8.21, 4.06))$. THE COLUMN LABELLED 'REFERENCE' LISTS THE SOURCE FOR THE BULGE+DISK DECOMPOSITION.

by the photometric decompositions. The dashed line showing $M_\bullet/M_{\bullet,\mathrm{pred}} = \Gamma_{\bullet,\mathrm{phot}}^{-1}$ represents the location of SMBHs that form on the $M_\bullet - \sigma_e$ relation and do not grow as the disk regrows. The dotted line instead shows the case $M_\bullet/M_{\bullet,\mathrm{pred}} = 1$, corresponding to SMBHs that always stay on the $M_\bullet - \sigma_e$ relation as the disk regrows. Most galaxies are above or near the dotted line, and this is especially true at $\Gamma_{\bullet,\mathrm{phot}} > 3$, regardless of whether the Gültekin et al. (2009) or the Beifiori et al. (2009) sample is considered. For the galaxy with the largest predicted $\Gamma_{\bullet,\mathrm{phot}}$, NGC 4594, we also plot the improved $M_\bullet$ measurement of Jardel et al. (2011) together with its uncertainty. NGC 4594 provides the greatest leverage in distinguishing how SMBHs and disks co-evolve; Figure 15 shows clearly that its SMBH continued to grow while its disk was forming. Galaxies would have followed the dashed line in Figure 15 if the $M_\bullet - M_{\mathrm{bul}}$ had been the more fundamental scaling relation rather than the $M_\bullet - \sigma_e$ relation, as assumed here.

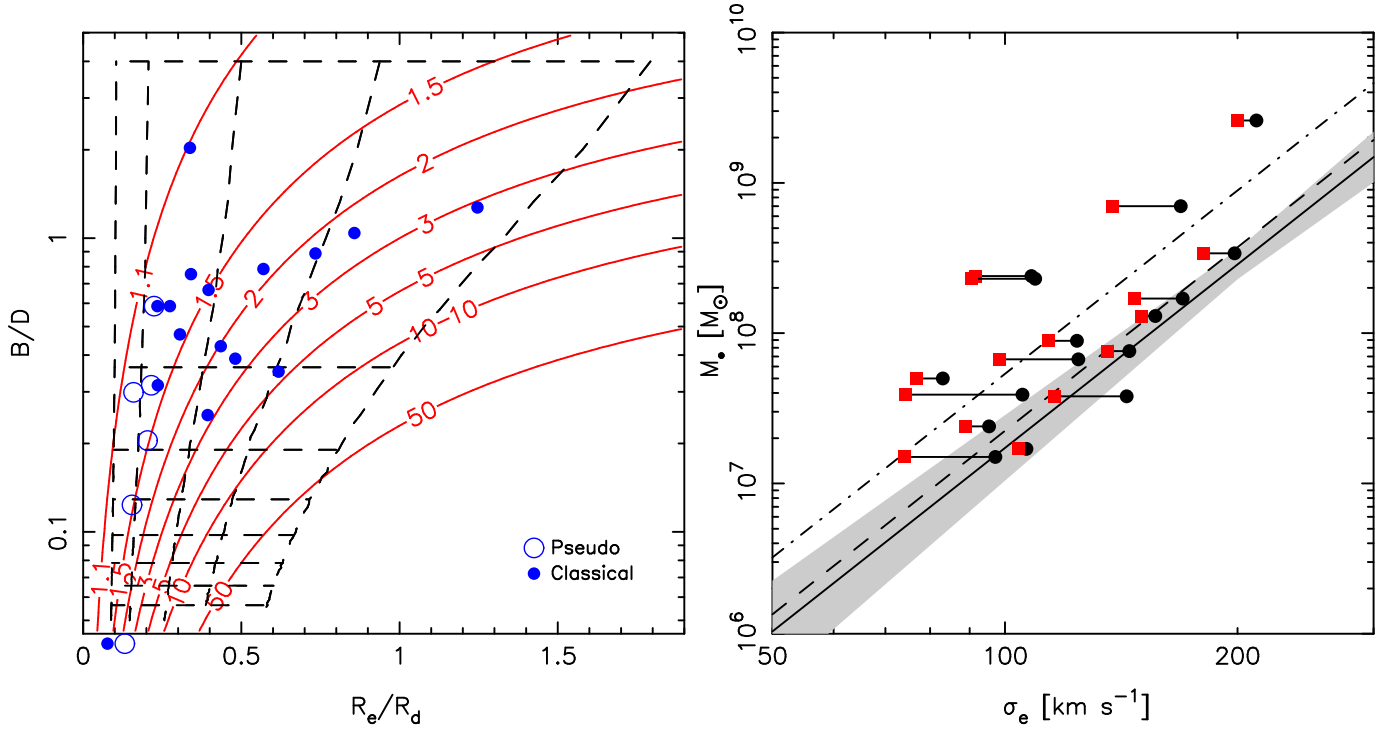There is a hint that barred galaxies are more frequently

FIG. 14.— The sample of galaxies with upper limits on $M_\bullet$ from Beifiori et al. (2009). Left panel: Distribution of the sample in the B/D-R_e/R_d plane. Filled symbols show $n > 2$ (classical) bulges while open symbols show $n < 2$ (pseudo) bulges. Contours of $\Gamma_\bullet$ assume $\beta = 4.24$ (Gültekin et al. 2009). Right panel: The $M_\bullet - \sigma_e$ relation of the 16 classical bulges. All black hole masses are upper limits only. The (black) circles with larger values mark the observed σ_e while the connected (red) squares show $\sigma_{e,0}$ (i.e., the decompressed values) from the fit of Eqn. 9. The various lines show our fits of the $M_\bullet - \sigma_e$ relation to different samples with the slope of the relation held fixed to that for elliptical galaxies in the Gültekin et al. (2009) sample ($\beta = 4.06$). The solid line shows the fit to the ellipticals ($\alpha = 8.46 \pm 0.10$), the dashed line fits the observed classical bulges ($\alpha = 8.57 \pm 0.10$) and the dot-dashed line the decompressed classical bulges ($\alpha = 8.95 \pm 0.11$). The shaded region shows the one sigma uncertainty on the $M_\bullet - \sigma_e$ relation of ellipticals.
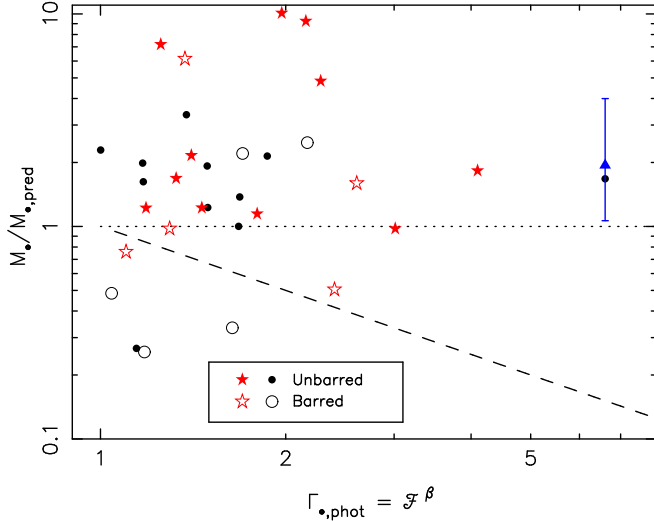

FIG. 15.— The residuals from (our fit for) the $M_\bullet - \sigma_e$ relation for ellipticals ($\alpha = 8.21$ for the Gültekin et al. (2009) sample and $\alpha = 8.46$ for the Beifiori et al. (2009) sample, with $\beta = 4.06$ for both) versus $\Gamma_\bullet$ predicted by the photometric decompositions. Barred and unbarred galaxies are shown as open and filled symbols, respectively. The (black) circles are SMBHs from Gültekin et al. (2009) while $\Gamma_\bullet$ is computed using the bulge+disk decomposition of Fisher & Drory (2010) (see text for details). The (red) stars are SMBH upper limits from the sample of Beifiori et al. (2009), with decompositions from Beifiori et al. (2012). The (blue) triangle with error bars shows NGC 4594 (the Sombrero galaxy) with improved $M_\bullet$ measurement taken from Jardel et al. (2011). The dashed line shows $M_\bullet/M_{\bullet,pred} = \Gamma_\bullet^{-1}$ while the dotted line shows $M_\bullet/M_{\bullet,pred} = 1$.

found near or below the dashed line in Figure 15, although this is not true of all barred galaxies. However the data do not reach $\Gamma_{\bullet,phot}$ values large enough to determine whether there is a real difference between barred and unbarred galaxies.

6. DISCUSSION AND CONCLUSIONS

Observations find that the peak of the integrated AGN activity is at $z \simeq 2$ (Wolf et al. 2003). The majority of bright quasars are in elliptical galaxies (Kukula et al. 2001; Dunlop et al. 2003; Kauffmann et al. 2003) but intermediate brightness Seyfert AGN, which represent a significant fraction of the total AGN number density at $z = 1.5 - 3$ (Ueda et al. 2003), are preferentially in disk galaxies (Schawinski et al. 2011). Schawinski et al. (2011) estimate that $23 - 40\%$ of SMBH growth in these AGN occur during a slow, secular mode of the type envisaged here. For the samples of disk galaxies with classical bulges that we explored here we estimate a mean $M_\bullet$ growth by $\sim 50\% - 65\%$. If instead we consider the samples with $M_\bullet$ measurements (both the direct and upper limits only) we find growth factors $\sim 60\% - 80\%$ from their photometric decompositions. The growth factor may be somewhat larger still if disks are steeper than exponential at their centers. Nonetheless, our estimated growth factor spans a range that is broadly in agreement with observational estimates.

We failed to find a significant difference between the $M_\bullet - \sigma_e$ relation of ellipticals and of classical bulges. With currently available samples this result is statistically significant only at about two-three sigma. Besides

increasing the sample size, the best future prospects for improving the significance of this result is if more galaxies with photometrically predicted large values of $\Gamma_\bullet$ were to have their $M_\bullet$ measured. We have provided a list of 5 galaxies (Table 3) with $\Gamma_\bullet \geq 3$; of these 4 have no directly measured $M_\bullet$. Galaxies with such large predicted growth factors offer excellent probes of the co-evolution of SMBHs and disks. Moreover Eqn. 9 makes it easy to trawl through photometric catalogs to search for further examples of galaxies with large predicted growth factors.

Since this paper was first submitted there have been several updates to the Gültekin et al. (2009) sample used in this work. We explored the impact of these via the sample compiled in McConnell & Ma (2012). The main changes for elliptical galaxies were updates of some SMBH masses and σ_e's and the addition of SMBH measurements in several brightest cluster galaxies (BCGs). Because BCGs evolve differently, we exclude these new galaxies from our sample and use the same sample as listed above under the Gültekin et al. (2009) sample, updating to the new $M_\bullet$ and σ_e values (dropping NGC 2778 which does not have a significant SMBH detection in recent measurements). For this sample we obtain $(\alpha, \beta) = (8.37 \pm 0.07, 4.39 \pm 0.42)$. The McConnell & Ma (2012) sample includes a number of new SMBH measurements in disk galaxies; at present we cannot determine whether any of these galaxies host classical bulges. In any case, several of these are low mass galaxies and are likely to host pseudo bulges, so we continue to fit to the same classical bulge sample from Gültekin et al. (2009) as before, now fixing the slope to $\beta = 4.39$. We obtain an intercept $\alpha = 8.32 \pm 0.09$, which is statistically indistinguishable from the value for ellipticals. Instead the value for the decompressed bulges is $\alpha = 8.51 \pm 0.11$, one sigma different from the value for ellipticals. We conclude that the latest measurements continue to show no evidence of an offset between ellipticals and classical bulges.

Assuming our result continues to hold with increased sample size, the consequence of our finding is that SMBHs grow along with disks. The main parameter regulating their growth is then the potential within which they reside, which is largely set by the bulge. This means that SMBH growth is self-regulated (e.g. Treister et al. 2011): SMBHs can grow until their feedback unbinds any gas otherwise destined to accrete onto them. This picture accounts also for the absence of correlations with properties of the dark matter halo or of the disk (Kormendy & Bender 2011; Kormendy et al. 2011).

Disk mass growth leads to an evolution of σ_e that is non-hierarchical, thereby adding nothing to the mass of a classical bulge. Another consequence of the absence of an offset in the $M_\bullet - \sigma_e$ relation of classical bulges therefore is that the bulge mass, which does not change as D/B increases, is not the main parameter determining $M_\bullet$. Thus the $M_\bullet - M_{bul}$ relation cannot be as fundamental as the $M_\bullet - \sigma_e$ relation. One interpretation of SMBH scaling relations views them as reflecting only a central-limit-theorem non-causal evolution produced by repeated galaxy merging (Peng 2007; Jahnke & Macciò 2011). In this picture the main correlation is between $M_\bullet$ and M_{bul}, both of which grow during mergers. Peng (2007) even predicted that bulge-dominated galaxies will have tighter scaling relations than disk-dominated ones. The lack of an offset between ellipticals and classical

bulges is contrary to this scenario: some form of regulation between SMBHs and bulges is required.

6.1. *The Milky Way Galaxy*

Whether the Milky Way hosts a classical or pseudo bulge remains unclear. While its bulge stars are mostly old, metal-rich and α-enhanced, favoring fast formation during mergers (McWilliam & Rich 1994; Zoccali et al. 2004, 2006, 2008; Lecureur et al. 2007; Fulbright et al. 2007), kinematics and morphology favor its formation via the central bar (Fux (1997, 1999); Shen et al. (2010) but see also Saha et al. (2012)). Assuming it is a classical bulge, the green star in the right panel of Figure 11 represents the Milky Way based on a bulge+disk decomposition of the density model of Bissantz & Gerhard (2002) (D/B = 8.3, $R_d/R_e = 3.2$); this implies $\Gamma_\bullet \simeq 3.7$. If currently $M_\bullet = 4.1 \times 10^6\ M_\odot$ (Ghez et al. 2008; Gillessen et al. 2009), the original SMBH would have had $M_\bullet \sim 1.1 \times 10^6\ M_\odot$ if it formed on the $M_\bullet - \sigma_e$ relation.

6.2. *Summary*

Our main results can be summarized as follows:

1. When a disk forms and grows around a pre-existing bulge, it gravitationally compresses the bulge, causing its effective velocity dispersion, σ_e, to increase. We have provided a fitting formula, Eqn. 9, for the change in σ_e for given bulge-to-disk mass and size ratios.

2. Using the SDSS data of Gadotti (2009) and Gadotti & Kauffmann (2009), we find evidence that classical bulges have been compressed as disks reformed around them. The photometric samples predict that bulges should experience a mean increase in σ_e by $\sim 10\%$. While small, the steepness of the $M_\bullet - \sigma_e$ relation requires SMBHs to grow, on average, by $\sim 50\%$ and extends to $> 200\%$.

3. The weak correlations between D/B and σ_8 and between R_d/R_e and σ_8 ensure that the main effect of bulge compression on the $M_\bullet - \sigma_e$ relation, if $M_\bullet$ remains unchanged as the disk regrows, is an offset to a smaller zero-point at fixed slope. The predicted offset between ellipticals and classical bulges is measureable with available samples of $M_\bullet$.

4. We do not find an offset between the $M_\bullet - \sigma_e$ relations of ellipticals and of classical bulges in either the sample of Gültekin et al. (2009) or that of Beifiori et al. (2009). Using available photometric decompositions of the galaxies, we show that an offset should have been found if $M_\bullet$ had not changed since the bulges formed. *Thus SMBHs must have grown along with disks.*

5. We estimate that SMBHs had to have grown by $\sim 50\% - 80\%$ in order to remain on the $M_\bullet - \sigma_e$ relation. Such significant SMBH growth is in agreement with recent observations that find that at $1.5 \leq z \leq 3$ SMBHs in disk galaxies grow by $\sim 23\% - 40\%$.

6. We have provided a list of 5 galaxies (Table 3) for which the SMBH is predicted to have needed

to grow by a factor greater than three to remain on the $\mathrm{M_\bullet} - \sigma_e$ relation. SMBHs with such large growth factors provide strong constraints on the mechanisms regulating the $\mathrm{M_\bullet} - \sigma_e$ relation and we strongly encourage measurement of their black hole masses.

APPENDIX

UNPUBLISHED PHOTOMETRIC FITS

We make use of unpublished decompositions of disk galaxies in the sample of Gültekin et al. (2009) kindly provided to us by David Fisher. Most of these decompositions have been published (Fisher & Drory 2008, 2010, 2011). However a few remain unpublished and we provide here a description of the analysis method by which David Fisher derived these decompositions.

The decompositions use archival *HST* and ground-based data. When possible, near infrared data are used as they are less sensitive to the obscuring effects of dust. Fisher & Drory (2008) show that for relative quantities, such as B/T, there is little difference from V-band to H-band; data are therefore restricted to be V-band or redder. For each galaxy the surface brightness profile is determined through ellipse fitting of both *HST* and ground-based data, thereby simultaneously constraining both the small scale structure at the center of the galaxy and the shape of the outer disk profile. Interfering objects, such as foreground stars and background galaxies, are masked via automatic source identification methods and manually removed. For ground-based images the sky is removed by subtracting a surface, fitted to regions of images that do not contain galaxy light. The radial sizes of the ellipses are optimized to maintain a roughly constant signal-to-noise ratio across the profile, and zero-point shifts of the ground-based image to match the *HST* data ensured continuity. The bulge+disk decompositions are then determined by fitting a Sérsic bulge plus outer exponential disk to the major axis surface brightness profile.

REFERENCES

Adams, F. C., Graff, D. S., Mbonye, M., & Richstone, D. O. 2003, ApJ, 591, 125
Adams, F. C., Graff, D. S., & Richstone, D. O. 2001, ApJ, 551, L31
Aller, M. C., & Richstone, D. O. 2007, ApJ, 665, 120
Andredakis, Y. C. 1998, MNRAS, 295, 725
Araya Salvo, C., Mathur, S., Ghosh, H., Fiore, F., & Ferrarese, L. 2012, ArXiv e-prints
Athanassoula, E. 2005, MNRAS, 358, 1477
Baes, M., Buyle, P., Hau, G. K. T., & Dejonghe, H. 2003, MNRAS, 341, L44
Barnes, J. E. 2012, ArXiv e-prints
Barway, S., & Kembhavi, A. 2007, ApJ, 662, L67
Baugh, C. M., Cole, S., & Frenk, C. S. 1996, MNRAS, 283, 1361
Begelman, M. C., Volonteri, M., & Rees, M. J. 2006, MNRAS, 370, 289
Beifiori, A., Courteau, S., Corsini, E. M., & Zhu, Y. 2012, MNRAS, 419, 2497
Beifiori, A., Sarzi, M., Corsini, E. M., Dalla Bontà, E., Pizzella, A., Coccato, L., & Bertola, F. 2009, ApJ, 692, 856
Bissantz, N., & Gerhard, O. 2002, MNRAS, 330, 591
Böker, T., Stanek, R., & van der Marel, R. P. 2003, AJ, 125, 1073
Bower, R. G., Benson, A. J., Malbon, R., Helly, J. C., Frenk, C. S., Baugh, C. M., Cole, S., & Lacey, C. G. 2006, MNRAS, 370, 645
Bower, R. G., Lucey, J. R., & Ellis, R. S. 1992, MNRAS, 254, 601
Bullock, J. S., Kolatt, T. S., Sigad, Y., Somerville, R. S., Kravtsov, A. V., Klypin, A. A., Primack, J. R., & Dekel, A. 2001, MNRAS, 321, 559
Bureau, M., & Freeman, K. C. 1999, AJ, 118, 126
Burkert, A., & Silk, J. 2001, ApJ, 554, L151
Chokshi, A., & Turner, E. L. 1992, MNRAS, 259, 421
Ciotti, L. 1991, A&A, 249, 99
Cisternas, M., et al. 2011, ApJ, 726, 57

Combes, F., Debbasch, F., Friedli, D., & Pfenniger, D. 1990, A&A, 233, 82
Combes, F., & Sanders, R. H. 1981, A&A, 96, 164
Courteau, S., de Jong, R. S., & Broeils, A. H. 1996, ApJ, 457, L73
Crenshaw, D. M., Kraemer, S. B., Boggess, A., Maran, S. P., Mushotzky, R. F., & Wu, C.-C. 1999, ApJ, 516, 750
Croton, D. J., et al. 2006, MNRAS, 365, 11
de Francesco, G., Capetti, A., & Marconi, A. 2006, A&A, 460, 439
de Grijs, R., & van der Kruit, P. C. 1996, A&AS, 117, 19
de Jong, R. S., & van der Kruit, P. C. 1994, A&AS, 106, 451
de Vaucouleurs, G. 1948, Annales d'Astrophysique, 11, 247
Debattista, V. P., Carollo, C. M., Mayer, L., & Moore, B. 2004, ApJ, 604, L93
Debattista, V. P., Carollo, C. M., Mayer, L., & Moore, B. 2005, ApJ, 628, 678
Debattista, V. P., Moore, B., Quinn, T., Kazantzidis, S., Maas, R., Mayer, L., Read, J., & Stadel, J. 2008, ApJ, 681, 1076
Debattista, V. P., & Sellwood, J. A. 2000, ApJ, 543, 704
Di Matteo, T., Springel, V., & Hernquist, L. 2005, Nature, 433, 604
Drory, N., & Fisher, D. B. 2007, ApJ, 664, 640
Dunlop, J. S., McLure, R. J., Kukula, M. J., Baum, S. A., O'Dea, C. P., & Hughes, D. H. 2003, MNRAS, 340, 1095
Dutton, A. A. 2009, MNRAS, 396, 121
Eggen, O. J., Lynden-Bell, D., & Sandage, A. R. 1962, ApJ, 136, 748
Erwin, P., Beltrán, J. C. V., Graham, A. W., & Beckman, J. E. 2003, ApJ, 597, 929
Erwin, P., & Gadotti, D. A. 2012a, Advances in Astronomy, 2012
Erwin, P., & Gadotti, D. A. 2012b, Advances in Astronomy, 2012
Fan, X., et al. 2004, AJ, 128, 515
Fan, X., et al. 2006, AJ, 131, 1203
Fan, X., et al. 2000, AJ, 120, 1167
Ferrarese, L. 2002, ApJ, 578, 90

Ferrarese, L., et al. 2006, ApJ, 644, L21
Ferrarese, L., & Merritt, D. 2000, ApJ, 539, L9
Fisher, D. B., & Drory, N. 2008, AJ, 136, 773
Fisher, D. B., & Drory, N. 2010, ApJ, 716, 942
Fisher, D. B., & Drory, N. 2011, ApJ, 733, L47
Fisher, D. B., Drory, N., & Fabricius, M. H. 2009, ApJ, 697, 630
Freeman, K. C. 1970, ApJ, 160, 811
Fulbright, J. P., McWilliam, A., & Rich, R. M. 2007, ApJ, 661, 1152
Fux, R. 1997, A&A, 327, 983
Fux, R. 1999, A&A, 345, 787
Gadotti, D. A. 2009, MNRAS, 393, 1531
Gadotti, D. A., & Kauffmann, G. 2009, MNRAS, 399, 621
Gebhardt, K., et al. 2000, ApJ, 539, L13
Ghez, A. M., et al. 2008, ApJ, 689, 1044
Gillessen, S., Eisenhauer, F., Trippe, S., Alexander, T., Genzel, R., Martins, F., & Ott, T. 2009, ApJ, 692, 1075
Graham, A. W. 2003, AJ, 125, 3398
Graham, A. W. 2008, ApJ, 680, 143
Graham, A. W., & Driver, S. P. 2007, ApJ, 655, 77
Greene, J. E., et al. 2010, ApJ, 721, 26
Gültekin, K., et al. 2009, ApJ, 698, 198
Haehnelt, M. G., & Kauffmann, G. 2000, MNRAS, 318, L35
Häring, N., & Rix, H.-W. 2004, ApJ, 604, L89
Hartmann, M., Debattista, V. P., Seth, A., Cappellari, M., & Quinn, T. R. 2011, MNRAS, 418, 2697
Hasinger, G., Miyaji, T., & Schmidt, M. 2005, A&A, 441, 417
Hernquist, L., & Mihos, J. C. 1995, ApJ, 448, 41
Hopkins, P. F., et al. 2010, ApJ, 715, 202
Hopkins, P. F., Hernquist, L., Cox, T. J., Di Matteo, T., Robertson, B., & Springel, V. 2006, ApJS, 163, 1
Hopkins, P. F., Hernquist, L., Cox, T. J., Robertson, B., & Krause, E. 2007a, ApJ, 669, 45
Hopkins, P. F., Hernquist, L., Cox, T. J., Robertson, B., & Krause, E. 2007b, ApJ, 669, 67
Hu, J. 2008, MNRAS, 386, 2242
Islam, R. R., Taylor, J. E., & Silk, J. 2003, MNRAS, 340, 647
Jahnke, K., & Macciò, A. V. 2011, ApJ, 734, 92
Jardel, J. R., et al. 2011, ApJ, 739, 21
Johansson, P. H., Naab, T., & Burkert, A. 2009, ApJ, 690, 802
Kauffmann, G., et al. 2003, MNRAS, 346, 1055
Kauffmann, G., White, S. D. M., & Guiderdoni, B. 1993, MNRAS, 264, 201
Kazantzidis, S., Abadi, M. G., & Navarro, J. F. 2010, ApJ, 720, L62
Kazantzidis, S., Magorrian, J., & Moore, B. 2004, ApJ, 601, 37
Kazantzidis, S., et al. 2005, ApJ, 623, L67
King, A. 2003, ApJ, 596, L27
King, A. R., & Pringle, J. E. 2006, MNRAS, 373, L90
Kocevski, D. D., et al. 2012, ApJ, 744, 148
Kormendy, J. 1977, ApJ, 218, 333
Kormendy, J., & Bender, R. 2011, Nature, 469, 377
Kormendy, J., Bender, R., & Cornell, M. E. 2011, Nature, 469, 374
Kormendy, J., & Kennicutt, R. C. 2004, ARA&A, 42, 603
Kormendy, J., & Richstone, D. 1995, ARA&A, 33, 581
Koushiappas, S. M., Bullock, J. S., & Dekel, A. 2004, MNRAS, 354, 292
Kukula, M. J., Dunlop, J. S., McLure, R. J., Miller, L., Percival, W. J., Baum, S. A., & O'Dea, C. P. 2001, MNRAS, 326, 1533
Lacey, C., & Cole, S. 1993, MNRAS, 262, 627
Lecureur, A., Hill, V., Zoccali, M., Barbuy, A., Gómez, A., Minniti, D., Ortolani, S., & Renzini, A. 2007, A&A, 465, 799
Leigh, N., Böker, T., & Knigge, C. 2012, MNRAS, 424, 2130
Lodato, G., & Natarajan, P. 2006, MNRAS, 371, 1813
Lynden-Bell, D. 1969, Nature, 223, 690
Madau, P., & Rees, M. J. 2001, ApJ, 551, L27
Magorrian, J., et al. 1998, AJ, 115, 2285
Marconi, A., & Hunt, L. K. 2003, ApJ, 589, L21
Markwardt, C. B. 2009, in Astronomical Society of the Pacific Conference Series, Vol. 411, Astronomical Data Analysis Software and Systems XVIII, ed. D. A. Bohlender, D. Durand, & P. Dowler, 251
Mayer, L., Kazantzidis, S., Escala, A., & Callegari, S. 2010, Nature, 466, 1082
McConnell, N. J., & Ma, C.-P. 2012, ArXiv e-prints

McConnell, N. J., Ma, C.-P., Gebhardt, K., Wright, S. A., Murphy, J. D., Lauer, T. R., Graham, J. R., & Richstone, D. O. 2011, Nature, 480, 215
McLaughlin, D. E., King, A. R., & Nayakshin, S. 2006, ApJ, 650, L37
McWilliam, A., & Rich, R. M. 1994, ApJS, 91, 749
Merritt, D., & Ferrarese, L. 2001a, MNRAS, 320, L30
Merritt, D., & Ferrarese, L. 2001b, ApJ, 547, 140
Miller, M. C., & Hamilton, D. P. 2002, MNRAS, 330, 232
Miralda-Escudé, J., & Kollmeier, J. A. 2005, ApJ, 619, 30
Mullaney, J. R., et al. 2012a, ApJ, 753, L30
Mullaney, J. R., et al. 2012b, MNRAS, 419, 95
Murray, N., Quataert, E., & Thompson, T. A. 2005, ApJ, 618, 569
Navarro, J. F., Frenk, C. S., & White, S. D. M. 1996, ApJ, 462, 563
Nelan, J. E., Smith, R. J., Hudson, M. J., Wegner, G. A., Lucey, J. R., Moore, S. A. W., Quinney, S. J., & Suntzeff, N. B. 2005, ApJ, 632, 137
Norman, C. A., Sellwood, J. A., & Hasan, H. 1996, ApJ, 462, 114
Nowak, N., Thomas, J., Erwin, P., Saglia, R. P., Bender, R., & Davies, R. I. 2010, MNRAS, 403, 646
Oh, S. P., & Haiman, Z. 2002, ApJ, 569, 558
Peng, C. Y. 2007, ApJ, 671, 1098
Pizzella, A., Corsini, E. M., Dalla Bontà, E., Sarzi, M., Coccato, L., & Bertola, F. 2005, ApJ, 631, 785
Portegies Zwart, S. F., & McMillan, S. L. W. 2002, ApJ, 576, 899
Raha, N., Sellwood, J. A., James, R. A., & Kahn, F. D. 1991, Nature, 352, 411
Robertson, B., Hernquist, L., Cox, T. J., Di Matteo, T., Hopkins, P. F., Martini, P., & Springel, V. 2006, ApJ, 641, 90
Rossa, J., van der Marel, R. P., Böker, T., Gerssen, J., Ho, L. C., Rix, H.-W., Shields, J. C., & Walcher, C.-J. 2006, AJ, 132, 1074
Saha, K., Martinez-Valpuesta, I., & Gerhard, O. 2012, MNRAS, 421, 333
Salucci, P., Szuszkiewicz, E., Monaco, P., & Danese, L. 1999, MNRAS, 307, 637
Sazonov, S. Y., Ostriker, J. P., Ciotti, L., & Sunyaev, R. A. 2005, MNRAS, 358, 168
Schawinski, K., Simmons, B. D., Urry, M., Treister, E., & Glikman, E. 2012, ArXiv e-prints
Schawinski, K., Treister, E., Urry, C. M., Cardamone, C. N., Simmons, B., & Yi, S. K. 2011, ApJ, 727, L31
Scott, N., & Graham, A. W. 2012, eprint arXiv:1205.5338
Searle, L., & Zinn, R. 1978, ApJ, 225, 357
Sellwood, J. A. 1983, Journal of Computational Physics, 50, 337
Sellwood, J. A. 2003, ApJ, 587, 638
Sérsic, J. L. 1968, Atlas de galaxias australes (Cordoba, Argentina: Observatorio Astronomico, 1968)
Shen, J., Rich, R. M., Kormendy, J., Howard, C. D., De Propris, R., & Kunder, A. 2010, ApJ, 720, L72
Silk, J., & Rees, M. J. 1998, A&A, 331, L1
Simmons, B. D., et al. 2012, ArXiv e-prints
Simonneau, E., & Prada, F. 2004, Revista Mexicana de Astronomia y Astrofisica, 40, 69
Soltan, A. 1982, MNRAS, 200, 115
Spitzer, L. J. 1942, ApJ, 95, 329
Springel, V., Di Matteo, T., & Hernquist, L. 2005a, ApJ, 620, L79
Springel, V., Di Matteo, T., & Hernquist, L. 2005b, MNRAS, 361, 776
Stadel, J. G. 2001, Ph.D. Thesis, University of Washington
Steinmetz, M., & Navarro, J. F. 2002, New Astronomy, 7, 155
Thomas, D., Maraston, C., Bender, R., & Mendes de Oliveira, C. 2005, ApJ, 621, 673
Treister, E., Natarajan, P., Sanders, D. B., Urry, C. M., Schawinski, K., & Kartaltepe, J. 2010, Science, 328, 600
Treister, E., Schawinski, K., Urry, C. M., & Simmons, B. D. 2012, ArXiv e-prints
Treister, E., Schawinski, K., Volonteri, M., Natarajan, P., & Gawiser, E. 2011, Nature, 474, 356
Tremaine, S., et al. 2002, ApJ, 574, 740
Tremaine, S. D., Ostriker, J. P., & Spitzer, L., Jr. 1975, ApJ, 196, 407
Ueda, Y., Akiyama, M., Ohta, K., & Miyaji, T. 2003, ApJ, 598, 886
van den Bosch, F. C. 1998, ApJ, 507, 601
van der Kruit, P. C., & Searle, L. 1982, A&A, 110, 79

Villalobos, Á., Kazantzidis, S., & Helmi, A. 2010, ApJ, 718, 314

Volonteri, M., Haardt, F., & Madau, P. 2003, ApJ, 582, 559

Volonteri, M., & Natarajan, P. 2009, MNRAS, 400, 1911

Volonteri, M., & Rees, M. J. 2005, ApJ, 633, 624

Wechsler, R. H., Bullock, J. S., Primack, J. R., Kravtsov, A. V., & Dekel, A. 2002, ApJ, 568, 52

Wehner, E. H., & Harris, W. E. 2006, ApJ, 644, L17

Weinzirl, T., Jogee, S., Khochfar, S., Burkert, A., & Kormendy, J. 2009, ApJ, 696, 411

Wolf, C., Wisotzki, L., Borch, A., Dye, S., Kleinheinrich, M., & Meisenheimer, K. 2003, A&A, 408, 499

Wolf, J., Martinez, G. D., Bullock, J. S., Kaplinghat, M., Geha, M., Muñoz, R. R., Simon, J. D., & Avedo, F. F. 2010, MNRAS, 406, 1220

Wyithe, J. S. B., & Loeb, A. 2003, ApJ, 595, 614

York, D. G., et al. 2000, AJ, 120, 1579

Younger, J. D., Hopkins, P. F., Cox, T. J., & Hernquist, L. 2008, ApJ, 686, 815

Zheng, W., et al. 2000, AJ, 120, 1607

Zheng, X. Z., et al. 2009, ApJ, 707, 1566

Zoccali, M., et al. 2004, A&A, 423, 507

Zoccali, M., Hill, V., Lecureur, A., Barbuy, B., Renzini, A., Minniti, D., Gómez, A., & Ortolani, S. 2008, A&A, 486, 177

Zoccali, M., et al. 2006, A&A, 457, L1